Vivianite is a key sink for phosphorus in sediments of the Landsort Deep, an intermittently anoxic deep basin in the Baltic Sea

Authors:

Nikki Dijkstra, Utrecht University, Netherlands[1] (mail: N.Dijkstra@uu.nl)

Caroline P. Slomp, Utrecht University, Netherlands[1] (mail: C.P.Slomp@uu.nl)

Thilo Behrends, Utrecht University, Netherlands[1] (mail: T.Behrends@uu.nl)

Expedition 347 Scientists

[1]Department of Earth Sciences - Geochemistry, Faculty of Geosciences, Utrecht University, Utrecht, The Netherlands

Corresponding author: Nikki Dijkstra

Postal address:

Postbus 80.021

3508 TA UTRECHT

The Netherlands

Published in Chemical Geology:

Available online since 27 May 2016

doi:10.1016/j.chemgeo.2016.05.025

Key words:

Integrated Ocean Drilling Program, Baltic Sea Basin Paleoenvironment, Landsort Deep, Phosphorus burial, Vivianite, Shelf-to-basin shuttle

Highlights

- We combine solid-phase geochemistry and micro-analysis to study P burial phases
- Brackish/marine sediments from the Landsort Deep contain Mn- and Mg-rich vivianite
- Vivianite may be formed in sediments below hypoxic, anoxic and likely sulfidic waters
- Shelf-to-basin shuttling of Fe and Mn is a key driver for vivianite formation

Graphical abstract

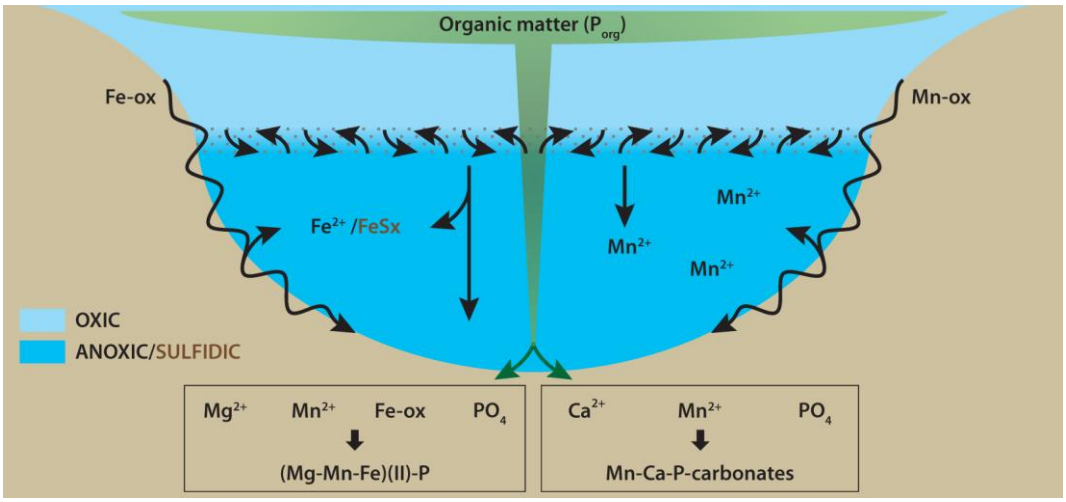

Abstract

Phosphorus (P) is an essential nutrient for marine organisms. Its burial in hypoxic and anoxic marine basins is still incompletely understood. Recent studies suggest that P can be sequestered in sediments of such basins as reduced iron(Fe)-P but the exact phase and the underlying mechanisms that lead to its formation are unknown. In this study, we investigated sediments from the deepest basin in the Baltic Sea, the Landsort Deep (site M0063), that were retrieved during the Integrated Ocean Drilling Project (IODP) Baltic Sea Paleoenvironment Expedition 347. The record comprises the whole brackish/marine Littorina Sea stage including past intervals of extensive hypoxia in the Baltic Sea that occurred during the Holocene Thermal Maximum (HTM_{HI}) and the Medieval Climate Anomaly ($MCA1_{HI}$ and $MCA2_{HI}$). Various redox proxies (e.g. the presence of laminations and high Mo contents) suggest almost permanent bottom water hypoxia during the Littorina Sea stage in the Landsort Deep. The bottom waters were likely even seasonally anoxic or sulfidic during the $MCA1_{HI}$ and $MCA2_{HI}$, and permanently sulfidic during the HTM_{HI}. With the use of micro-analysis of sieved minerals (SEM-EDS, XRD and synchrotron-based XAS), we show that Mn- and Mg-rich vivianite crystals are present at various depths in the Littorina Sea sediments. We also have strong indications for vivianite in the $MCA1_{HI}$, $MCA2_{HI}$ and HTM_{HI} deposits. The formation of vivianite thus likely explains the high Fe-bound P fraction throughout the whole Littorina Sea stage. Shuttling of Fe and Mn from the shelves into the basin and high inputs of P in settling organic matter are likely key drivers for vivianite formation. Our study shows that vivianite can likely form in near-surface sediments under a broad range of bottom water redox conditions, varying from hypoxic and anoxic to sulfidic.

1. Introduction

Bottom water hypoxia (i.e. oxygen concentrations below 2 mg/l) is a growing problem in marine waters worldwide, and a well-known cause of the death of benthic organisms (Diaz and Rosenberg, 2008). The development of these so-called "dead zones" is in most cases the result of enhanced external inputs of nutrients into coastal waters. The nutrients may be responsible for increased primary production in the water column and the associated elevated flux of organic matter to the seafloor may then result in an oxygen demand in bottom waters that outpaces supply (Diaz and Rosenberg, 2008).

Phosphorus (P) is a key nutrient for life on earth (Tyrrell, 1999). Enhanced P availability in the water column can therefore increase marine primary productivity and play an important role in the development of bottom water hypoxia in marine systems. Burial in sediments is the only removal pathway for P from the marine environment (Froelich et al., 1982; Ruttenberg, 2003). This P burial pool mainly consists of a mixture of organic P, authigenic Ca-P (e.g. carbonate-fluorapatite), iron(Fe)-bound P, exchangeable P and detrital P (e.g. Ruttenberg, 2003). The contribution of these P pools to total P burial is, in part, controlled by the redox conditions in the deeper water column and surface sediments upon deposition (Ingall et al., 1993; Slomp and Van Cappellen, 2007).

Organic P is often a major P burial pool in sediments that are overlain by hypoxic, anoxic or sulfidic bottom waters, as is also observed in surface sediments from the Baltic Sea (e.g. Jilbert et al., 2011; Mort et al., 2010). This is thought to be the combined result

of an increased input of organic matter from the productive water column in such settings and enhanced preservation of organic matter (including some P) in sediments under anoxic conditions, e.g. due to the slower kinetics of anaerobic degradation of organic matter and the lack in capability of anaerobic bacteria to oxidize certain organic compounds (Canfield, 1994; De Lange et al., 2008; Hartnett et al., 1998; Moodley et al., 2005; Raiswell and Canfield, 2012; Tsandev et al., 2012). The burial of organic P in hypoxic and anoxic systems is counteracted, however, by preferential release of organic P relative to organic carbon (C_{org}) (Ingall and Jahnke, 1994; Ingall et al., 1993). This has been attributed to the production of phosphatases by carbon-limited microbes, which leads to the removal of PO_4 groups from organic molecules, thereby facilitating the uptake of the remaining organic carbon (Steenbergh et al., 2013, 2011). Given that the released PO_4 cannot be retained by anaerobic bacteria, sedimentary C_{org}/P_{org} ratios in sediments overlain by hypoxic or anoxic bottom waters are generally elevated relative to 106, the Redfield C_{org}/P_{org} ratio for marine organic matter (Gächter et al., 1988; Ingall and Jahnke, 1997; Ingall et al., 1993; Jilbert et al., 2011; Van Cappellen and Ingall, 1994).

In many marine settings, P released from organic matter is retained in the surface sediment through sorption to Fe-oxides (e.g. Slomp et al., 1996). This Fe-oxide bound P is, however, typically an insignificant P fraction in sediments that are overlain by anoxic or sulfidic bottom waters since dissimilatory Fe(III) reduction and dissolution of Fe-oxides by reaction with hydrogen sulfide (HS^-) generally remove all reactive Fe-oxides (Canfield et al., 1992). The lack of Fe-P recycling in surface sediments below anoxic bottom waters may limit the accumulation of porewater phosphate (mainly HPO_4^{2-} in seawater; henceforth termed PO_4) in some systems and may hamper the subsequent

formation and burial of authigenic apatite-P at depth (Reed et al., 2011b; Ruttenberg and Berner, 1993; Slomp et al., 1996). Authigenic apatite-P may still form in sediments in anoxic basins, where the highly productive surface waters in these marine zones provide a large input of degradable organic matter (including organic P) to the underlying sediments, thereby supporting a sink-switching of organic P to authigenic Ca-P (Ruttenberg, 2003). Recently, it has been demonstrated that authigenic Ca-P is a major P sink in organic-rich sediments in the anoxic and sulfidic deep basin of the Black Sea (Dijkstra et al., 2014). In anoxic sediments that are low in PO_4, however, apatite formation can be negligible (Reed et al., 2011a). Also other factors, such as porewater alkalinity, fluoride and calcium (Ca^{2+}) concentrations, may play a role in the formation of authigenic apatite-P (Ruttenberg, 2003). Although P-bearing minerals can thus still form in sediments overlain by a hypoxic or anoxic water column, they are often characterized by ratios of organic carbon to total P (C_{org}/P_{tot}) above the Redfield ratio of 106, illustrating that P released by organic matter degradation is generally not fully retained through authigenic mineral formation (Algeo and Ingall, 2007).

Recent studies for the Black Sea, Baltic Sea and Chesapeake Bay show that brackish/marine sediments which are (intermittently) overlain by anoxic or sulfidic bottom waters may be enriched in Fe-bound P (Dijkstra et al., 2014; Jilbert et al., 2011; Li et al., 2015). In all three systems, this P burial pool accounted for more than 20% of the total sedimentary P pool. The Fe-bound P fraction was quantified with the citrate-dithionite-bicarbonate(CDB)-step of the sequential P extraction (SEDEX; Ruttenberg, 1992). This extraction scheme does not differentiate between Fe-oxide bound P and Fe(II)-phosphates such as vivianite ($(Fe_3PO_4)_2.8H_2O$) (e.g. Nembrini et al., 1983).

Although some Fe-oxides may survive transport through a low oxygen water column, the burial of Fe-oxide bound P is generally assumed to be low in sediments overlain by anoxic or sulfidic bottom waters (Jilbert and Slomp, 2013a; Mortimer, 1941; Reed et al., 2015). The Fe-bound P fraction in such sediments may thus represent Fe(II)-phosphates. In the Baltic Sea, distinct Fe and P enrichments with a mean Fe/P ratio of 1.65 (as quantified with scanning electron microscope energy dispersive spectroscopy (SEM-EDS)) were observed in the Fårö Deep, an intermittently sulfidic deep basin in the Baltic Sea. Given the similarity to the Fe/P ratio of vivianite (1.5), the enrichments were suggested to consist of vivianite (Jilbert and Slomp, 2013a). Synchrotron-based X-ray absorption spectroscopy (XAS) of Chesapeake Bay surface sediments also point towards the presence of vivianite in sediments overlain by seasonally hypoxic or anoxic bottom waters (Li et al., 2015). At present, the exact phase and composition of the Fe(II)-phosphates are unknown, as are the underlying mechanisms that lead to their formation and their fate upon long-term burial in hypoxic, anoxic or sulfidic basins.

In this study, we present a sediment record (0 – 90 mbsf) from the Landsort Deep that was retrieved during the Integrated Ocean Drilling Program (IODP) Baltic Sea Paleoenvironment Expedition 347. This record comprises the whole brackish Littorina Sea stage including three intervals of extensive hypoxia/anoxia that occurred during the Holocene Thermal Maximum (ca 8000–4000 yrs ago) and the Medieval Climate Anomaly (ca 750–1000 yrs ago; Zillén et al., 2008). We have combined porewater analyses, solid-phase geochemistry (total elemental composition, sequential extractions for Fe, sulfur(S) and P) and micro-analysis of sieved aggregates (SEM-EDS and synchrotron-based XAS) to demonstrate the presence of magnesium(Mg)- and manganese(Mn)-rich vivianite in sediments that were deposited during the Littorina Sea stage. Our study

shows that Fe-bound P, in the form of vivianite, is a major P burial phase in the Landsort Deep.

2. Methods

2.1 Study area and site

The Baltic Sea has been subject to variations in salinity after the retreat of the last Weichselian ice sheet (Andrén et al., 2011; Björck, 1995). The deglaciation resulted in the formation of the Baltic Ice Lake around 16 kyr BP. Afterwards, the Baltic Ice Lake became connected to the ocean and the Yoldia Sea developed (around 11.7 kyr). The next stage, the Ancyclus Lake, began after the isolation of the Yoldia Sea. The first brackish inflows into this freshwater lake were recorded at 9.8 kyr (Andrén et al., 2000; Berglund et al., 2005), marking the onset of a gradual transition towards more brackish/marine conditions. The current Littorina Sea was established around 7 kyr BP (Sohlenius et al., 2001). Sediment records of molybdenum (Mo), which is a proxy for the presence of HS^- near the sediment-water interface (Erickson and Helz, 2000), and C_{org} have been used to identify hypoxic intervals that occurred during the Holocene Thermal Maximum and the Medieval Climate Anomaly in the Gotland Basin and Fårö Deep (Jilbert and Slomp, 2013b; Lenz et al., 2014; Zillén et al., 2008). Jilbert and Slomp (2013b) further indicate that multiple hypoxic events can be distinguished during the Holocene Thermal Maximum (HTM_{HI}) whereas the hypoxic interval during the Medieval Climate Anomaly appears to consist of two main events (i.e. $MCA1_{HI}$ and $MCA2_{HI}$).

At present, the water column of the Baltic Proper (Fig. 1) is permanently stratified with an upper layer of brackish water with salinities of 7–8 and more saline

deep waters of 11–13 (Conley et al., 2009). The Baltic Proper today experiences widespread hypoxia and severe cyanobacteria blooms since the 1950's, which are related to excess nutrient loading from agriculture and waste water (Carstensen et al., 2014; Funkey et al., 2014; Gustafsson et al., 2012).

The main deep basins of the Baltic Proper are located in the northern region of the Baltic Proper (water depth = 437m; Fig. 1). The Landsort Deep is the deepest basin of the whole Baltic Sea. Long sediment cores were retrieved from five holes (hole A – E) in the central part of the Landsort Deep (M0063; 58°37.34′N, 18°15.25′E) during the IODP Baltic Sea Paleoenvironment Expedition 347 in 2013.

2.2 Core description

The visual core description was conducted during the sampling party in the Bremen Core Repository and is described in Andrén et al (2015). A simplified version of the lithology is shown in figure 2. The lower part of the sediment record consists of a ~50 m thick grey/greyish brown layer of clays that were deposited on diamicton during the Baltic Ice Lake stage. These sediments are overlain by a thin layer of brackish deposits around 45 m sediment depth that were likely deposited during the brackish phase of the Yoldia Sea stage. The grey sediments that are observed between 30 and 40 m sediment depth were probably deposited during the Ancyclus Lake stage (Andrén et al., 2015). The shift towards more organic-rich and laminated sediments between 25.5 and 30 m sediment depth indicates the transition from the Ancyclus Lake to the Littorina Sea stage in the sediment record (A/L-transition). The higher salinities also lead to the first appearances of foraminifera at 30 m sediment depth and a shift in

diatom assemblages from freshwater to brackish/marine taxa between 27 and 25.5 m sediment depth (Andrén et al., 2015). The upper 25 m of the sediment record consists of laminated organic-rich black clays. Two intervals with more prominent laminations are observed in the sediment record between 17.4 to 25.2 m and 4.1 to 6.7 m.

2.3 Organic carbon and total elemental concentrations

Sediment samples were taken directly after core recovery on board with 10 ml syringes ("onboard samples"; Hole E). These samples were stored in nitrogen(N_2)-purged aluminum(Al) bags at 4˚C (2 m resolution) to prevent sample oxidation and associated changes in Fe, S and P fractionation (Kraal and Slomp, 2014; Kraal et al., 2009). Three to five months after core retrieval, additional samples were taken on shore with plastic scoops at a 20 cm resolution ("onshore samples"; Hole C). The latter samples were also stored in N_2-purged Al-bags at 4˚C. All samples were freeze-dried and ground with an agate mortar and pestle at Utrecht University in a N_2-purged glovebox.

Subsamples (0.2 g) from all onboard samples and selected onshore samples were decalcified by two washes with hydrochloric acid (1 M HCl; 4 and 12 hours, respectively) and a final rinse with UHQ water (Santvoort et al., 2002). The decalcified samples were freeze-dried and analyzed with a CN analyser (Fisons Instruments NA 1500) to determine C_{org}. Based on laboratory reference materials and replicates, the relative error in C_{org} was generally less than 5%.

A sediment subsample (0.125 g) was digested overnight at 90 °C in a mixture of hydrofluoric acid, nitric acid and perchloric acid. This was done for all onboard and onshore samples. The acids were fumed off during the next day and the residue was

redissolved in 1 M HNO_3. The final solution was then analyzed for total S, Mo, Fe, Al, Mg, Mn, Ca and P using inductively coupled plasma optical emission spectrometry (ICP-OES; Perkin Elmer Optima 3000). The relative error, based on analyses of laboratory reference material (ISE-921) and sample triplicates, was generally less than 3%.

2.4 Porewater

Porewater was sampled from the cores immediately after recovery, using either rhizon samplers or squeezers (0.2 µm pore size; see Andrén et al., 2015). Salinity was determined by optical refraction (OR) (Krüss Optromic Digital Refractometer DR 6300). The salinity was also calculated based on the chloride (Cl^-) concentrations as determined with the Metrohm 882 Compact Ion Chromatography at the University of Bremen. Comparison between both methods can reveal the contribution of other dissolved salts than typically present in seawater. Decomposition of organic matter can for instance lead to an enrichment of cations and alkalinity in porewaters (e.g. Wallmann et al., 2008). Alkalinity was determined by single-point titration according to Grasshoff et al. (1983). The method of Hall and Aller (1992) was used to measure ammonium (NH_4^+) by flow injection analysis including gas membrane for ammonia extraction and conductivity detection. The total P, Fe, Mg and Mn content of filtered (0.2 µm) and acidified (10 µL of conc. HNO_3 per mL) porewater samples were measured using ICP-OES (Agilent Technologies 700 Series) and are assumed to represent PO_4, Fe^{2+}, Mg^{2+} and Mn^{2+}. For further details, we refer to Andrén et al. (2015).

2.5 Sequential extractions

2.5.1 Iron extraction

A dry sediment subsample (0.1 g) of the onboard samples was subjected to the sequential Fe extraction method as developed by Poulton and Canfield (2005). First, the carbonate-associated Fe (Fe-carb) was targeted with 1 M sodium acetate brought to pH 4.5 with acetic acid for 24 h. We then applied an extraction with 1 M hydroxylamine-HCl in 25% v:v acetic acid for 48 h to extract the amorphous Fe-oxide fraction (Fe-ox1). Afterwards, crystalline Fe-oxides were targeted with a 50 g/L sodium dithionite solution buffered to pH 4.8 with 0.35 M acetic acid/0.2 M sodium citrate for 2 hours (Fe-ox2). Finally, a 0.2 M ammonium oxalate/0.17 M oxalic acid solution targeted magnetite (Fe-mag; 2h). All extractions were performed at room temperature in an argon-filled glovebox with argon-purged solutions to prevent further oxidation artefacts (Kraal and Slomp, 2014; Kraal et al., 2009). Fe concentrations were determined colorimetrically using the 1,10-phenanthroline method (APHA, 2005). Based on replicates and in-house standards, relative errors were generally less than 10%. Note that the Fe-ox1 fraction may be overestimated as some extracted Fe might in fact represent FeS (e.g. Egger et al., 2014).

2.5.2 Sulfur extraction

We applied the S extraction method as developed by Burton et al. (2008) on subsamples (0.5 g) to determine acid volatile sulfide (AVS) and chromium-reducible sulfide (CRS). The HS^- in AVS and CRS was converted into hydrogen sulfide gas (H_2S) with a 6 M HCl/0.1 M ascorbic acid solution and an acidic chromium(II) solution, respectively. Afterwards, the H_2S was trapped in an alkaline zinc (Zn) acetate solution. The amount of sulfide in the ZnS precipitate was then measured by iodometric titration

(APHA, 2005). The AVS fraction is assumed to represent iron monosulfides (FeS) but might also consist of Mn sulfides, an important mineral phase in the Landsort Deep (Lepland and Stevens, 1998). The CRS fraction is assumed to represent pyrite (FeS_2). Both solutions were purged with N_2 prior to the extraction. To shield the sediment samples from oxygen, the AVS step was performed in an argon-filled glovebox and the CRS step was conducted underneath a nitrogen gas line. The relative error based on triplicates was 6% for AVS and 3% for CRS.

2.5.3 Phosphorus extraction

The SEDEX method (Ruttenberg, 1992), as modified by Slomp et al. (1996), but including the exchangeable P step was applied to ground sediment subsamples (0.1 g) of the onboard samples to determine the different P phases in the sediments. Two subsamples (0.05 g) of a vivianite standard (as synthesized according to Dijkstra et al., 2014; Rouzies et al., 1993) were also subjected to the extraction scheme. The exchangeable P fraction was determined by an extraction with a magnesium chloride solution (1M $MgCl_2$ brought to pH 8 with sodium hydroxide) for 0.5 h. The Fe-bound P content was then targeted by extraction with a solution of 0.3 M trisodium citrate and 25 g/L sodium dithionite buffered to pH ~ 7.6 in 1 M sodium bicarbonate (CDB solution) for 8 h, followed by a wash step with 1 M $MgCl_2$ for 0.5 h. The subsample residue was then extracted with 1 M sodium acetate buffered to pH 4 with acetic acid (6 h) to determine the authigenic Ca-P content, again followed by a 1 M $MgCl_2$ wash step for 0.5 hour. Detrital P was extracted with 1 M HCl for 24 h and, finally, organic P was targeted with a 1 M HCl extraction for 24 h after combusting the subsample residue at 550 °C for 2 hours. Only the P concentrations in the CDB extracts were determined by ICP-OES. The P

concentrations in all other extracts were determined colorimetrically on a Shimadzu spectrophotometer with the molybdenum blue method (Strickland and Parsons, 1972). The first five steps were conducted in a nitrogen-purged glovebox with nitrogen-purged solutions. To increase the sample resolution, we also performed the same P extraction on a selection of the onshore samples. All handling of the onshore samples until the first HCl extraction was performed beneath a nitrogen gas line in order to shield the samples from oxygen. Although the onshore samples were collected a few months after core recovery, we did not observe differences between the P fractionation of the onboard and onshore samples. We therefore assume that no major changes in P fractionation occurred in the onshore samples due to oxidation artefacts. The sum of the sequential P fractions over the whole cores was similar to the total P concentrations as derived from the ICP-OES (generally < 15% difference). All extractions were performed at room temperature and relative errors were generally less than 10% (based on sample triplicates and in-house standards).

2.6 Sieving method and SEM-EDS of vivianite crystals

Sediment samples for sieving (5 – 30 cc) were taken from every core catcher and mid-way between the core catcher, resulting in an overall sample resolution of about 1.5 m (Andrén et al., 2015). Examination of sieved sediment with a light microscope revealed the presence of blue aggregates (>63 μm). The blue color is a characteristic oxidation artifact of phosphates from the vivianite group (e.g. Nriagu, 1972; Yakubovich et al., 2001). This mineral group exists of minerals with the common formula $M_3(TO_4)_2.8H_2O$, where M represents Fe, Mg, Zn, Ni, Co and T represents P or As. For simplicity, we will collectively refer to this group of phosphate minerals as pure vivianite

$(Fe(II)_3(PO_4)_2.8H_2O$, the pure Fe-phosphate from the vivianite group (excluding arsenates).

Blue aggregates from 3 depths (1.6 m (Hole B), 12.7 m (Hole E) and 27.4m (Hole D) were mounted on an Al stub and coated with platinum. These aggregates were then analyzed by SEM-EDS (JCM 6000PLUS NeoScope Benchtop SEM) with 15 kV accelerating voltage in scanning electron mode. In addition, SEM-EDS was performed in the 0-20 keV energy range for elemental quantification (probe current: 1 nA; acquisition time: 50 seconds). SEM-EDS software was used to estimate the relative abundances in mol% for the major elements (P, Fe, Mn, Mg, Silica (Si) and Al). Other elements such as Ca and potassium (K) generally accounted for less than 1 % of the molar mass and were not included in the calculation.

The extent of the penetration beam into the particles depends on the particle density and the accelerating voltage (Casuccio et al., 2004). Casuccio et al. (2004) calculated that an electron beam with a high accelerating voltage could only penetrate 5 µm into particles with a density nearly similar to vivianite. The beam may thus be incapable of reaching the inner part of the aggregates and we therefore assume that the SEM-EDS analysis determines the elemental distribution of the aggregate surfaces. One-way analysis of variance (ANOVA) tests with a Shapiro-Wilk test for normality (P = 0.05) and a post-hoc Tukey test were performed in Sigmaplot 12.3 to compare the relative elemental abundances between the aggregates from different depths.

2.7 X-ray diffraction (XRD) & elemental composition of a blue aggregate

We used XRD to investigate the mineralogy of a blue aggregate from 12.7 m and a ground vivianite standard (see Dijkstra et al. (2014) for synthesis). The vivianite crystal was ground with an agate mortar and pestle inside an argon-purged glovebox. Both

samples were stored in a N_2-purged jar prior to analysis. The XRD analysis was performed on a Bruker D2 diffractometer using Cobalt Kα radiation, over a 2θ range of 5-85° with a step size of 0.026° 2θ and a measurement time of 0.4 seconds per step. There was not enough material for bulk XRD analysis on the blue aggregates from sediment depths of 12.7 and 27.4 m.

After the XRD analyses, the ground aggregate (4 mg) was digested overnight at 90 °C in a mixture of hydrofluoric acid(HF), nitric acid (HNO_3) and perchloric acid. The acids were fumed off during the next day and the residue was redissolved in 1 M HNO_3. The final solution was then analyzed using ICP-OES (Perkin Elmer Optima 3000). We calculated the relative molar abundances for the major elements, i.e. P, Fe, Mn, Mg and Al (note that Si is lost during the HF-destruction). All other measured elements contributed less than 2% to the total molar mass of the aggregate.

2.8 XAS of blue aggregates and bulk sediments

Blue aggregates, bulk sediment samples and various standards were investigated with X-ray absorption spectroscopy at the beamlines BM26a (DUBBLE) and ID21 at the European Synchrotron Radiation Facility (ESRF) in Grenoble, France. The layouts of the beamlines are described in Borsboom and Bras (1998), Nikitenko and Beale (2008) and Salomé et al. (2013), respectively.

XAS measurements at the K-edges of Fe and Mn were performed at BM26a in the energy range 7.00 - 7.65 keV and 6.50 - 6.90 keV, respectively. Absorption spectra were collected at room temperature in fluorescence mode. Spectra were collected in June

2014 from a blue aggregate from 12.7 m sediment depth (Aggregate I) which was fixed with Kapton® tape before mounting on a holder and measurement.

In addition, another blue aggregate from the same depth (Aggregate II) was analyzed under vacuum at the ID21 beamline in April 2015 at the P K-edge in the energy range 2.13 - 2.40 keV as well as at the Fe K-edge in the energy range 7.00 - 7.65 keV. We also collected XAS spectra at the P K-edge on ground bulk sediment samples from 7.34 m and 20.83 m sediment depth. The aggregates and the ground material were sealed in Ultralene® film before installation into the sample holder of ID21. Spectra were collected at ID21 without using the KB mirror at room temperature in fluorescence mode.

The monochromator was calibrated against the maximum intensity of the first derivative of a Fe foil (7.11198 keV) or a tricalcium phosphate standard (2.14943 KeV) for XAS measurements of Fe and Mn or P, respectively. All individual spectra (2-16 spectra per sample) were merged to obtain average spectra. We used the ATHENA software package (Ravel and Newville, 2005) for background removal and normalization. The collected spectra were compared to XANES and EXAFS spectra of reference materials. The reference spectra were measured in the same or other experiments at the ID21 beamline in fluorescence mode (except fluorapatite: transmission mode) or they were obtained from literature (Table 1). Consistency in energy calibration was evaluated using spectra of reference materials which were included in the various spectra sets.

Results

3.1 Total sediment composition

Based on enrichments in sediment organic C, S and Mo, we identified the hypoxic interval during the Holocene Thermal Maximum (HTM_{HI}) and two hypoxic intervals that likely occurred during the Medieval Climate Anomaly ($MCA1_{HI}$ and $MCA2_{HI}$) in the sediments between 17.9-27.0 m, 9.5-11.0 m and 3.5-7.4 m, respectively (Fig. 2). Highest C_{org}, S and Mo concentrations are observed in the HTM_{HI} and the $MCA2_{HI}$ sediments. Sediments that were deposited during the hypoxic intervals are all enriched in Fe/Al, Mg/Al, Mn and Ca relative to the surrounding deposits. The highest Fe/Al and Mg/Al ratios are found in sediments that were deposited during the $MCA2_{HI}$. For Mn and Ca, the highest concentrations are observed in the sediments that were deposited just after the A/L-transition and in the $MCA2_{HI}$ sediments. Sediments that were deposited during the $MCA1_{HI}$ are lower in Fe/Al, Mn and Ca than sediments that were deposited during the other hypoxic intervals. Sediment P is highest in the sediments of the $MCA2_{HI}$ (130 µmol/g) but also high in sediments of the HTM_{HI} and $MCA1_{HI}$ (~70 µmol/g). The Littorina Sea sediments are characterized by high C_{org}/P_{tot} and C_{org}/P_{org} ratios relative to the underlying lacustrine deposits. The C_{org}/P_{org} ratio is particularly high in sediments of the HTM_{HI}, $MCA1_{HI}$ and $MCA2_{HI}$ (> 1000 mol/mol; 750 mol/mol and 750 mol/mol, respectively). No distinct differences in total sediment composition are observed between both holes (Hole C and E).

3.2 Porewater trends with sediment depth

The porewater composition in the Littorina Sea sediments is distinctly different from the porewater composition in the underlying deposits (Fig. 3; Hole A-E). The salinities are highest in the Littorina Sea deposits at 15 m sediment depth and decrease to <2 at 50 m sediment depth. The elevated salinities around 60 m are likely caused by

seawater contamination and do not represent in-situ salinities. Porewater Mg^{2+}, a major component of sea water salinity, shows an almost similar porewater trend with maximum values of 28 mmol/L. The higher OR-based salinity than Cl^--based salinity is indicative for a higher abundance of other dissolved ions than typically observed in seawater, such as NH_4^+ and PO_4. These products of organic matter decomposition are indeed highest in the Littorina Sea sediments with maximum values of 60 mmol/L for alkalinity, 10 mmol/L for NH_4^+ and 1.6 mmol/L for PO_4. Porewater NH_4^+ and PO_4 are low in all sediments below 35 m sediment depth (<0.1 mmol/L). The dissolved Fe concentrations vary strongly with low values in the sediments that were deposited during the HTM_{HI} and $MCA2_{HI}$ (1-20 µmol/L) and maximum values in the lake sediments just below the A/L-transition (>400 µmol/L). No Fe^{2+} is detected in the deeper lake sediments (> 60 m). Porewater Mn^{2+} is also elevated in the Littorina Sea sediments, in particular in the upper 5 m of sediments and in sediments between the MCA_{HI} and HTM_{HI} deposits.

3.3 Iron, sulfur and phosphorus fractionation

The sum of the extracted Fe phases generally accounts for ~ 30 % of the total Fe content throughout the core, with the exception of the sediments that were deposited during the HTM_{HI} (~ 15 %), the $MCA1_{HI}$ (~ 60 %) and the upper 3 m of the sediments (>40%; Fig. 4). The sediments that were deposited during the HTM_{HI} are low in Fe-carbonates, amorphous Fe-oxides and more crystalline Fe-oxides whereas sediments of the $MCA1_{HI}$ and $MCA2_{HI}$ are slightly enriched in these Fe fractions. Magnetite is low throughout the upper 30 m of sediment. The sediments just below the A/L-transition are enriched in Fe-carbonates while Fe-carbonates are nearly absent deeper in the core. The

lacustrine sediments between 30 and 50 m contain less Fe-oxides than the deeper lacustrine sediments.

All Littorina Sea deposits contain some FeS and/or FeS_2 while the sediments below the A/L-transition barely contain any of these two S phases (Fig. 5). In the upper 30 m of sediment, FeS and FeS_2 account for ~ 70 % of the total S pool. The sediments that were deposited during the $MCA1_{HI}$ and $MCA2_{HI}$ are most enriched in FeS (> 200 µmol/g). The highest FeS_2 concentrations are observed in sediments from the upper section of the HTM_{HI} (> 700 µmol/g).

Authigenic Ca-P and Fe-bound P are both major P phases in the Littorina Sea sediments (Fig, 6). The sediments of the HTM_{HI} and $MCA2_{HI}$ are both enriched in authigenic Ca-P relative to the surrounding sediments. The Fe-bound P fraction is high (>40 µmol/g) in the sediments of the $MCA1_{HI}$ and $MCA2_{HI}$ and in the surface sediments (<1 mbsf). Organic P is a minor P fraction and generally follows the trend of Fe-bound P. Detrital and exchangeable P are low throughout the sediment record (<12 µmol/g). The synthesized vivianite standard dissolves completely in the CDB step of the SEDEX (> 99 % of total extracted P).

3.4 Crystal morphology, XRD and elemental composition

Blue aggregates that were found in the top 4 m of sediment (1.6-3.9 m), between the sediments of the $MCA1_{HI}$ and HTM_{HI} (12.7 m), and in the A/L-transition (27.4 m) vary in size and morphology (Fig. 7). The crystals in the upper 4 m of sediment are small (<100 µm) and are platy and/or needle-shaped (Fig 7A). In contrast, large blue aggregates where recovered from the sediment from 12.7 m (>800 µm; Fig, 7B). The

blue spherical aggregates from 27.4 m are slightly smaller in diameter (~ 400 μm; Fig, 7C).

The X-ray diffractogram of the crystal from 12.7 m sediment depth is almost identical to the diffractogram of the measured vivianite standard (Fig. 7D). Main diffraction peaks for the aggregate are located at 15.4, 13.1, 35.2 and 21.2 and 38.6 °2θ Co K-α and agree in position and relative intensity to those of vivianite. In comparison to the synthesized vivianite standard, some diffraction peaks of the aggregate are shifted to the right by about 0.1-0.2 °2θ. This may be caused by the incorporation of Mn as similar shifts have been observed in Mn-rich vivianite (Egger et al., 2015a; Nakano, 1992).

The aggregate from 12.7 m sediment depth consists of P and almost equal amounts of Fe, Mn, Mg, resulting in a mean (Fe,Mn,Mg)/P ratio of 1.6 (Table 2). According to EDS analysis, the minerals tend to have higher (Fe,Mn,Mg)/P–ratios (Table 2). This discrepancy between the ICP-OES and EDS results can be attributed to two phenomena: 1) a bias of the SEM-EDS analysis of bulk materials towards heavier elements and 2) the fact that SEM-EDS predominately probes the aggregate surface. In the latter case, the discrepancy could reflect a surface coating rich in Fe, Mn and/or Mg, as observed on vivianite crystals in cold-seep sediments (Hsu et al., 2014).

The relative abundance of Fe, Mn and Mg at the mineral surfaces differs significantly between crystals from different depths ($p<0.05$). For instance, Fe is significantly more abundant at the surfaces of crystals from 1.6 and 27.4 m than at the surfaces of crystals from 12.7 m sediment depth (>50 mol% versus 21 mol%). In addition, the surfaces of the vivianite crystals from 1.6 m sediment contain more Mn

than the surfaces of the other crystals (28 mol% versus >11 mol%) and Mg is only a major surface element for crystals from 12.7 m sediment depth (20 mol%). The presence of some Si and Al in samples from 12.7 and 27.4 m likely reflects clay particles that were not removed during sieving.

3.5 XANES and EXAFS spectra

The Fe XANES spectra of the aggregates from 12.7 m sediment depth (aggregate I and II) are almost identical to the XANES spectrum of the vivianite reference (Fig. 8). Characteristic features of the vivianite XANES spectrum, which are resembled in the spectra of the aggregates, are the positions of the edge and white line as well as the shoulder at 7130 eV and the hump around 7140 eV. The amplitudes and shapes of these features in the spectra of the blue aggregates and the vivianite standard also show great similarities. Also the Fe EXAFS spectra of aggregate I and vivianite are similar up to k-values of about 9 Å and exhibit the same characteristic oscillations.

When comparing the Mn XANES spectrum of aggregate I with those of the Mn(II) and Mn(III) phosphates, hureaulite and $MnPO_4$, the position of the edge indicates that Mn occurs predominately in the form of Mn(II) in the aggregates. The similarity of the sample spectrum with that of hureaulite further suggests that the Mn coordination environments are alike. The Mn EXAFS spectrum resembles that of Fe indicating that Mn(II) replaces Fe(II) in the vivianite structure in the blue aggregates

Also the XANES spectrum for P from the aggregate from 12.7 m sediment depth (Aggregate II) confirms that vivianite is the predominant phase in the blue aggregates. The P-XANES spectrum matches the spectrum of vivianite in Figure 8D. The white line is

positioned at 2153.3 eV. The XANES spectrum of the blue aggregate has similar features as the vivianite spectrum, including the post-edge oscillations with maxima at 2158, 2164 and 2179 eV.

The XANES spectra of bulk sediment samples do not give direct indications for the presence of vivianite. The amplitude of the white line is higher compared to that in the spectra of all P-reference materials. Also the position of the maximum at 2153.2 eV is slightly lower compared to vivianite (0.1-0.2 eV) and the characteristic oscillations between 2155 and 2167 eV are missing. The spectra do not correspond closely to any of the analyzed reference materials and they might reflect a combined signal from various P phases including adsorbed P. Deconvolution of the spectra by linear combination fitting of the P XANES spectra collected in fluorescence mode is, however, problematic due to the strong effect of self-absorption.

4. Discussion

4.1 The Landsort Deep is an intermittently anoxic brackish/marine basin

Trends in porewater salinity, which are also affected by downward diffusion, confirm the brackish conditions in the upper 30 m of sediment, just after the A/L-transition (Fig. 3). The higher salinity resulted in a density stratified water column which likely contributed to the development of hypoxic conditions in the deeper waters of the Landsort Deep (Lepland and Stevens, 1998). Episodic inflows of oxygenated North Sea water only resulted in short periods of oxygenation in the bottom waters in the Landsort Deep (Fonselius, 1981; Matthäus and Nausch, 2003). In this low oxygen environment, bottom macro fauna did not establish and the subsequent lack of

bioturbation resulted in the continuous deposition of laminated sediments as observed at our site (Fig. 2; Andrén et al., 2015)

Concurrent changes in C_{org} and Mo in our sediment record can be attributed to changes in the bottom water redox conditions upon sediment deposition. The sedimentary C_{org} and Mo record therefore allowed us to identify three intervals when bottom waters were anoxic or sulfidic (HTM_{HI}, $MCA1_{HI}$ and $MCA2_{HI}$). The most prominent laminations in the sediment were observed in sediments from these intervals (Fig. 2). Sedimentary Mo can often also be used as a proxy for the degree of anoxia (Algeo and Lyons, 2006). This is however limited in strongly restricted basins. In such basins, reservoir effects can lead to the depletion of MoO_4^{2-} in the water column and limit Mo burial in the underlying sediments (Algeo and Lyons, 2006). Low Mo/C_{org} ratios, as observed in our sediments (~12.5 ppm/wt%; Supplementary information S1), are characteristic for strongly restricted basins. The almost identical enrichments in Mo in the HTM_{HI} and $MCA2_{HI}$ sediments (Fig. 3) may thus be the result of a Mo-depleted water column and not caused by a similar degree of anoxia during both periods. This is supported by the observation that sediments that were deposited in the less restricted Northern Gotland basin and Fårö Deep were indeed more enriched in Mo than the sediments in the Landsort Deep (Supplementary information S1; Jilbert and Slomp, 2013b).

In the Landsort Deep, other geochemical features in the sediment can therefore provide better insights in the degree of hypoxia during the hypoxic intervals. The

$MCA1_{HI}$ and $MCA2_{HI}$ sediments are for instance characterized by lower C_{org}/P_{org} ratios than the HTM_{HI} (Fig. 2). This may be indicative of less reducing bottom water conditions during the MCA_{HI} and $MCA2_{HI}$ compared to the HTM_{HI}. Some Fe-oxides may have survived the transport throughout the water column during the $MCA1_{HI}$ and $MCA2_{HI}$, explaining their presence in the sediment as Fe-ox1 and Fe-ox2 (Fig. 4). In contrast, most Fe-oxides may have been converted to FeS_2 in the sulfidic water column during the HTM_{HI}. This could explain the low Fe-oxide and high FeS_2 content in these sediments (Fig. 4 and 5). We conclude that the Landsort Deep was probably almost permanently sulfidic during the HTM_{HI} whereas the sediments that were deposited during the $MCA1_{HI}$ and $MCA2_{HI}$ were likely only seasonally overlain by anoxic or sulfidic bottom water. Also at the start of the $HTM_{HI,}$ the bottom waters may have been less sulfidic compared to the bottom water at the end of the HTM_{HI} (lower total S and FeS_2; Fig. 2 & Fig. 5). Trends in organic C, S, Mo and FeS_2 further suggest that the Landsort Deep was less productive and anoxic during the $MCA1_{HI}$ than during the $MCA2_{HI}$ (Fig. 2).

4.2 Vivianite is an important P burial sink in the Landsort deep

Blue aggregates were discovered in sieved sediment samples from several depths in the Littorina Sea sediments. With the use of various techniques (XRD and SEM-EDS), we demonstrate that these aggregates consist of Mn- and Mg-rich Fe-phosphates with a vivianite crystal structure (Table 2; Fig. 7). The (Fe,Mn,Mg)/P-ratio of an aggregate from 12.7 m sediment depth of 1.6 (Table 2) is also close to the stoichiometry of vivianite ((Fe,Mn,Mg)/P = 1.5) and further corroborates that these aggregates consist of vivianite. Although Mn or Mg-containing vivianite has been previously observed in freshwater and

marine sediments (e.g. Hsu et al., 2014), the crystals in our study are unusually enriched in both elements.

The P fraction in the SEDEX extraction that includes vivianite, termed Fe-bound P, is high throughout the sediment record (Fig. 6). However, no vivianite crystals were observed in sediments from the hypoxic intervals that occurred during the Littorina Sea stage. A possible explanation for the absence is that the crystals were too small to be detected (<63 μm) due to partial sulfidization of vivianite crystals upon burial. This is in accordance with a study in the Fårö Deep, where only small Fe- and P-rich particles (<10 μm) were observed in sediments that were overlain by sulfidic bottom water upon deposition (Jilbert and Slomp, 2013a).

Our XAS results also provide clear evidence that the blue aggregates contain Mn^{2+}-rich vivianite as the dominant Fe-, Mn- and P-bearing phase (Fig. 8). In contrast, the bulk P XANES spectra do not show the post-edge features that are characteristic for vivianite (Fig. 8E). This is likely because the measured fluorescence spectrum in heterogeneous samples can be biased towards the signature of P species at particle surfaces. The P XANES spectra may therefore reflect disperse, and presumably surface adsorbed, P in our sediments. Such bias towards adsorbed P may also explain the absence of post-edge oscillations in bulk P XANES spectra from vivianite-rich surface sediments in the Bothnian Sea (Egger et al., 2015a).

The presence of vivianite thus likely explains the high Fe-bound P content, as quantified with the CDB step of the SEDEX, throughout the Littorina Sea deposits (Fig. 6;

section 3.6). Similar to Fe-oxide bound P, vivianite is also extracted with the hydroxylamine-HCl step of the sequential Fe extraction (Dijkstra et al., 2014). However, the Fe/P stoichiometry of both Fe-bound P phases differs: while the Fe/P ratio (mol/mol) of pure vivianite is 1.5, the minimum Fe/P ratio of pure colloidal Fe-oxide bound P is assumed to be 2 (Dellwig et al., 2010; Thibault et al., 2009) and typical Fe/P ratios for Fe-oxides in marine sediments are close to 10 (Anschutz et al., 1998; Slomp et al., 1996). In oxic surface sediments in the Bothnian Sea, the ratio between hydroxylamine-HCl Fe and Fe-bound P was ~7 (Egger et al., 2015a). In most HTM_{HI} deposits, the hydroxylamine-HCl-extracted Fe/Fe-bound P-ratio is between 1.0 to 1.8 mol/mol, so close to the Fe/P stoichiometry for pure vivianite (Fig. S2). This supports our hypothesis that vivianite also can explain the Fe-bound P fraction in the HTM_{HI} deposits.

A higher Mn content in vivianite may reflect Mn supersaturation in reducing environments, resulting in the replacement of Fe by Mn. This has been suggested to occur in sediments in Lake Biwa (Nakano, 1992). The Fe/P ratios slightly below 1.5 might be attributed to the inclusion of Mg, and particularly, Mn in vivianite. The CDB (Fe+Mn)/P-ratios are always above 1.5 (Fig. S3), indicating that the CDB extracts contain sufficient Fe and Mn to explain all Fe-bound P as Mn-rich vivianite.

Biogenic apatite (fish debris) can partly dissolve in the CDB step of the SEDEX procedure and could thus lead to an overestimation of Fe-bound P in the sediment (Schenau and De Lange, 2000). This might explain the presence of Ca in our CDB extract from sediments from the HTM_{HI} (Fig. S3). Given that only very few fish fragments were observed during sediment sampling, we expect this to be a minor P burial phase in the

Landsort Deep. Fish debris were also found to be an unimportant P burial phase in the sulfidic surface sediments of the Landsort Deep (Mort et al., 2010). Some P adsorbed to calcite may also dissolve in the CDB step, as proposed by Jensen and McGlathery (1998). This is expected to be most relevant for calcite-rich deposits whereas the Littorina Sea sediments in the Landsort Deep are low in calcite (maximum calcite content is 6 wt%; Emelyanov, 2001). Most Ca in the Landsort Deep is likely buried in the form of Mn-Ca-carbonates and these Mn-Ca-carbonates do not dissolve in the CDB solution (Rutten and de Lange, 2003). We therefore conclude that the presence of vivianite likely explains most of the Fe-bound P in the HTM_{HI} sediments. Burial of vivianite may thus have occurred throughout the Littorina Sea stage under hypoxic, anoxic and likely also sulfidic bottom waters.

Authigenic Ca-P is also a major P burial phase in the Littorina deposits (Fig. 6). Part of the authigenic Ca-P burial can be explained by the pool of Mn-Ca-P-carbonates in the marine sediments in the Landsort Deep, as suggested in earlier studies (Carman and Rahm, 1997; Jilbert and Slomp, 2013a; Mort et al., 2010; Suess, 1979). These phosphates are believed to form in these deposits when phosphate substitutes for carbonate in the structure of Mn-carbonates (Suess, 1979). Some authigenic Ca-P may also represent other phosphates that dissolve in the acetate step of the SEDEX such as carbonate-fluorapatite, biogenic Ca-P and detrital Ca-P (Mort et al., 2010; Ruttenberg, 1992; Slomp et al., 2013). Apatite in spherical palynomorphs and other microfossils may for instance account for the background authigenic Ca-P pool in sediments from the Northern Gotland basin and Fårö Deep (~ 10 to 15 μmol/g P; Jilbert and Slomp, 2013a). Together

with Mn-Ca-P-carbonates and apatite species, vivianite can thus account for the high P burial pool in the Littorina Sea deposits (Fig. 2).

4.3 Organic P as an internal source for authigenic vivianite

The precipitation of vivianite in marine systems generally occurs within the sediments (Egger et al., 2015a; Hsu et al., 2014; Jilbert and Slomp, 2013a) and thus requires an internal supply of dissolved P in the sediments or bottom water. In the sediments of the Landsort Deep degradation of organic matter provides such a supply of dissolved P, and also releases other solutes such as NH_4^+ and alkalinity (Fig. 3).

The release of dissolved P in the sediment is further amplified by the preferential release of P relative to organic C from organic matter (Ingall and Jahnke, 1997; Ingall et al., 1993; Jilbert et al., 2011). We calculated that large amounts of P may have been released to the porewaters through this process, in particular from the $MCA2_{HI}$ deposits and HTM_{HI} deposits, where preferential release of P may have resulted in the release of more than 40 μmol/g P (Fig. S4). Our simple back-of-the-envelope calculation ignores any preferential P release in the water column (Faul et al., 2005; Loh and Bauer, 2000) but shows that this extra internal P source is sufficient to explain more than 50% of the P in the Fe-bound P fraction in the Littorina Sea sediments (Fig. S4). Although organic P only constitutes a minor P phase in the marine sediments of the Landsort Deep today (Fig. 6), it thus likely played an important role in the observed P mineral formation in the Landsort Deep. Organic P remineralization has been linked to the formation of other P-bearing minerals such as authigenic Ca-P (e.g. Ruttenberg and Berner, 1993), and a similar sink-switching mechanism may thus exist for vivianite. This could also lead to

the presence of organic remains in vivianite aggregates, a feature that is commonly observed in freshwater systems (see Rothe et al., (2016) for an overview).

4.4 The importance of the Fe shelf-to-basin shuttle for vivianite formation

Marine planktonic organic matter is too low in Fe to be an important sedimentary Fe source for vivianite in the Landsort Deep (C_{org}:Fe ratios can be as high as 100,000; Anderson and Morel, 1982). Hence, an alternative particle flux is required as a Fe source for vivianite precipitation.

We propose that the Landsort Deep experiences a weak shuttling of Fe from the shelf sediments to the deep basin throughout the complete Littorina Sea stage. This could explain the elevated Fe/Al content in the Littorina Sea sediments (0.70) relative to the detrital background of 0.6 – 0.65 (Fehr et al., 2008) (Fig. 2). Hypoxic basins as the Landsort Deep can receive Fe that is mobilized from surrounding shelf sediments. The released Fe can then undergo multiple cycles of re-oxidation, deposition and re-mobilization in the surface sediment before a portion of the Fe reaches the deep basin as nanoparticle Fe-oxides or complexed Fe^{3+} (Raiswell and Canfield, 2012; Scholz and Severmann, 2014; Wijsman et al., 2001). Only part of the Fe is directly converted to FeS_x in the surface sediments and the Fe-oxides that survive sulfidization can act as an internal Fe source in the sediments, explaining the presence of Fe^{2+} in the Littorina Sea deposits (Fig. 3).

This shelf-to-basin-shuttle of Fe in the Landsort Deep may have intensified during the HTM_{HI}, $MCA1_{HI}$ and $MCA2_{HI}$ when the bottom waters in the shelf region became more reducing and the subsequent enhanced release of Fe from these sediments

increased the flux of Fe-oxides or complexed Fe^{3+} through the oxic water column into the deep basin. Some Fe may also have been transported to the deep basin through the ferruginous layer in the redoxcline (Anderson and Raiswell, 2004; Eckert et al., 2013; Lewis and Landing, 1991; Lyons and Severmann, 2006). Part of the Fe that enters the deep basin may already be converted to FeS_x within the sulfidic water column (Reed et al., 2015). This increased trap efficiency and the elevated Fe flux from the shelves likely both contributed to the enhanced Fe/Al-burial during the HTM_{HI}, $MCA2_{HI}$, and to a lesser extent during the $MCA1_{HI}$.

The lower Fe/Al ratios in the HTM_{HI} deposits relative to the $MCA2_{HI}$ sediments can be explained by a difference in the ratio between the Fe source and basin sink area (S/B-ratio; Raiswell and Anderson, 2005). During the HTM_{HI}, most bottom waters from the shelf sediments were likely anoxic/sulfidic and subsequently acted as a sink for Fe (smaller S/B-ratio), resulting in a reduced Fe burial per surface area in the sink region. In contrast, the Fe source area during the $MCA2_{HI}$ may have been identical to the source area during most of the Littorina Sea stage (no change in S/B-ratio).

Some Fe-oxides that were transported from the shelf to the deep basins likely survived transport through the water column, even during the $MCA1_{HI}$ and $MCA2_{HI}$ when bottom waters were seasonally anoxic or sulfidic. This is expected because of the relatively shallow water depths in the Baltic Sea, which allow for relatively short travel times of Fe-oxides from oxic surrounding shelves to the anoxic and sulfidic deep basins and the known resistance of crystalline Fe oxides to rapid reductive dissolution by sulfide (Canfield et al., 1992). In the present-day Fårö Deep more crystalline deep Fe oxides are also thought to reach the surface sediments, as deduced both from sediment Fe-bound P profiles (Jilbert and Slomp, 2013a) and as assumed in a model

reconstruction of modern Fe shuttling in the same basin (Reed et al., 2015). The Fe-oxides may have acted as a source of reactive Fe for vivianite formation, and could explain the positive correlation between the degree of shelf-to-basin Fe shuttling, as indicated by sedimentary Fe/Al, and the Fe-bound P content in the upper part of our sediment record (R^2= 0.59; Fig. S5). Due to the intense Fe shelf-to-basin shuttle, the $MCA1_{HI}$ and $MCA2_{HI}$ sediments are also characterized by sedimentary S:Fe-reactive ratios below 1.5 (Fig. S6). This ratio between total S and reactive Fe in the sediments (as all Fe except silicates; S:Fe-reactive) can be used as a proxy for the occurrence of vivianite, whereby ratios below 1.5 are assumed to indicate that not all reactive Fe is captured as FeS_x and vivianite formation is favoured (Rothe et al., 2015).

The presence of crystalline Fe-oxides in the HTM_{HI} deposits (Fig. 4) suggests that some Fe-oxides also survived transport through the sulfidic water column during the HTM_{HI}. However, we do not observe a good correlation between sedimentary Fe/Al and the Fe-bound P content in the HTM_{HI} deposits (Fig. S5). The S:Fe-reactive ratios are also above 1.5 , which is the upper threshold for vivianite occurrence according to Rothe et al. (2015). As bottom waters were likely permanently sulfidic, vivianite may have formed in micro-environments in the sediments where S was in short supply relative to Fe, as suggested previously for the Fårö Deep sediments (Jilbert and Slomp, 2013a). Incorporation of Mn^{2+} and Mg^{2+} may have contributed to vivianite formation in these micro-environments in the absence of sufficient Fe^{2+}.

4.5 Sources of dissolved Mn and Mg in the Landsort Deep

The deep basin of the Landsort Deep acts as an efficient trap for Mn that is mobilized from the shelves and shuttled into the deep basin (Lenz et al., 2015; Lepland

and Stevens, 1998). This Mn shuttle leads to an accumulation of Mn^{2+} in the deeper water column. In the deep basin, most Mn is ultimately buried as Mn-carbonates that form from fresh Mn-oxides which precipitate after periodic inflows of oxygenated waters (Ganeshram et al., 2002; Huckriede and Meischner, 1996). The burial of Mn-carbonates in the Landsort Deep appears to be less dependent on oxygen inflows due to continuous supply of Mn-oxides into the deep basin through strong sediment focusing (Lenz et al., 2015). In addition, some Mn in the sediments in the Landsort Deep is buried as Mn sulfides (Lepland and Stevens, 1998; Suess, 1979). The shuttling of Mn has resulted in marine deposits rich in Mn, particularly those formed at the $MCA2_{HI}$ and the start of the HTM_{HI} and $MCA2_{HI}$ (Fig. 2). Precipitated Mn-Ca-carbonates in the Baltic Sea are assumed to be metastable (Jakobsen and Postma, 1989) as they fall within the wide miscibility gap between the two endmembers in the system $CaCO_3$–$MnCO_3$–H_2O (at 25 °C; Middelburg, 1987). These carbonates may thus undergo various dissolution and (re)precipitation cycles at depth, resulting in the internal Mn^{2+} source that we observe in the porewaters today (Fig. 3). This shelf-to-basin shuttle of Mn thus provides a Mn^{2+} pool in the Landsort Deep sediments that allows formation of Mn-rich vivianite. The enhanced Mn deposition may also have stimulated the precipitation of P as Mn-Ca-P-carbonates, as reflected by the concurrent trends in authigenic Ca-P and total Mn throughout the Littorina deposits (Fig. 2 and Fig. 6).

While the porewater P, Fe and Mn pools in the sediments are thus affected by particle fluxes towards the sediment and diagenesis, the porewater Mg^{2+} geochemistry in the Landsort Deep is mainly controlled by salinity (Fig. 2; Andrén et al., 2015). Only some Mg^{2+} is assumed to be released by desorption and exchange of Mg^{2+} and the weathering of silicate minerals (e.g. Wallmann et al., 2008). Whereas the porewater Mg^{2+}

pool may be a cation source for vivianite, the burial of Mg-rich vivianite is not a major Mg burial pool. For example, vivianite with an assumed Mg/P ratio of 0.5 could only account for ~10 % of the Mg in the $MCA2_{HI}$ deposits (total Mg content of 500 µmol/g). The twofold increase in Mg/Al during the $MCA2_{HI}$ thus likely resulted from the incorporation of Mg in the Mn-carbonate structure (proposed Mg/Mn-ratio of 17; Suess, 1979) and other cation exchange processes (e.g. Drever, 1971; von Breymann et al., 1990).

4.6 Diagenesis and vivianite burial in the Landsort Deep

Authigenic vivianite that forms at or just below the sediment water interface in the Landsort Deep may be diagenetically altered upon long-term burial. We hypothesize that the surfaces of the crystals may be subjected to continuous exchange of cations with the surrounding pore fluids after authigenesis. This may explain the high abundance of Mg at the surface of the aggregate from 12.7 m that coincides with the maximum of porewater Mg^{2+} (Table 2; Fig. 3). Also the highest surface enrichments in Fe and Mn are observed at a depth where Fe^{2+} and Mn^{2+} are abundant (1.6 m; Table 2; Fig. 3). Although surface uptake of dissolved cations involving solid solution formation is well established for carbonates (e.g. Stipp et al., 1992), studies on vivianite and the exchange of cations are still lacking.

The crystal morphology may also indicate diagenetic alternations of the vivianite minerals. The platy- and needle-shaped vivianite crystals from the upper 4 m of sediments (Fig. 7) likely represent freshly formed vivianite that has not been subject to major diagenetic alternation. Similar crystals were for instance observed in surface sediments in the Bothnian Sea (Egger et al., 2015a) and lake Ørn in Denmark (O'Connell

et al., 2015). In contrast, the less crystalline aggregates at 12.7 m (Fig. 7) are comparable to the vivianite concretions in ancient deposits in Lake Baikal, Russia (3.7 Myr; Sapota et al., 2006). We suggest that crystalline vivianite which forms in the surface sediment may evolve into these aggregates through diagenetic processes. One of these mechanisms is the partial dissolution with HS^-, which has previously been suggested to be the main cause of pitting of vivianite crystals in Lake Biwa in Japan (Murphy et al., 2001) and lake Ørn in Denmark (O'Connell et al., 2015). Such scavenging of Fe from the crystal surfaces may also explain the irregular shape of the aggregates from 12.7 m depth. How other diagenetic processes, such as crystal growth, affected the crystal morphology on the longer term is currently unknown as literature on the growth mechanism and kinetics of vivianite crystals in natural sediments is still limited (Rothe et al., 2016).

We propose that the spherical crystals observed at 27.4 m sediment depth (Fig. 7C) did not form in the surface sediments but, instead, formed diagenetically at depth at the A/L-transition. Such spherical vivianite aggregates are assumed to precipitate in organic-rich sediments in which PO_4 and Fe saturation is maintained during vivianite formation (Zelibor et al., 1988). This laboratory study suggests that the nucleation occurs on charged organic macromolecules with crystal growth proceeding in different directions from a common centre (Zelibor et al., 1988). Ancyclus lake deposits are enriched in Fe-oxides (Fig. 4; Böttcher and Lepland, 2000; Holmkvist et al., 2011), and reductive dissolution of these Fe-oxides just below the A/L-transition not only resulted in a lower Fe-oxide content in the upper Ancyclus Lake deposits than in the underlying sediments but also created an Fe^{2+} pool at depth in the Landsort Deep sediments (Fig. 3). The upward diffusing Fe^{2+} meets the downward diffusing PO_4 that is released by organic

matter degradation of the Littorina Sea deposits at the A/L-transition (Fig. 3). At this boundary, the porewaters are likely sufficiently enriched in Fe and P to stimulate the precipitation of the spherical vivianite that we observe in the sediments today. These crystals may be less altered by cation exchange processes due to the high Fe content in the pore fluids, resulting in vivianite crystals with outer parts rich in Fe (Table 2). The formation of vivianite may thus explain the small peak in Fe-bound P in the sediments at the A/L-transition (Fig. 6).

4.7 Relevance for P burial in hypoxic, anoxic or sulfidic brackish/marine basins

The formation of Mn- and Mg-rich vivianite and Mn-Ca-P-carbonates in the Landsort deep is likely controlled by shelf-to-basin shuttling of Fe and Mn and high organic matter fluxes towards the seafloor, as illustrated in Fig. 9. Similar mechanisms may also explain the high Fe-bound P and authigenic Ca-P content in the surface sediments of the Landsort Deep (Fig. 6; Mort et al., 2010). Recently, it has been suggested that a strong shelf-to-basin shuttling also enhanced the burial of Fe-P (presumably vivianite) in the anoxic Fårö Deep (Jilbert and Slomp, 2013a; Reed et al., 2015). This shuttling of Fe and/or Mn from shelf sediments is a world-wide phenomenon in brackish/marine systems, as shown for other basins in the Baltic Sea and for the Black Sea, the Orca Basin, the Effingham Inlet and the open ocean (Jilbert and Slomp, 2013a; Lenz et al., 2015; Lyons and Severmann, 2006; Raiswell and Anderson, 2005; Scholz and Severmann, 2014; Scholz et al., 2013). Apart from these modern marine systems, the P sequestration in deep basin sediments in the geological past may also have been affected by this shuttling mechanism, as recently suggested for Cambrian sediments (Creveling et al., 2014).

Shuttling of Fe and Mn can lead to a strong decoupling between the sedimentary C_{org}/P_{tot} ratios and the degree of anoxia upon deposition. In the Landsort Deep, sediments that were deposited during past intervals of hypoxia were at least twice as rich in P (relative to the surrounding sediments; Fig. 2). This is contrary to what is expected based on preferential release of P from organic matter under low-oxygen conditions (Ingall and Jahnke, 1997; Ingall et al., 1993). This illustrates that the specifics of depositional environments should be considered when using C_{org}/P_{tot} to reconstruct past redox-conditions in marine systems.

5. Conclusion

In this study, we found vivianite crystals rich in Mn and Mg in sediments that were deposited during the brackish/marine Littorina Sea stage in the Landsort Deep. These vivianite minerals likely formed in near-surface sediments overlain by hypoxic bottom waters. We also have indications that vivianite is present in sediments that were deposited when bottom waters at the Landsort deep were anoxic or even sulfidic. Vivianite minerals are a major burial P phase in the Landsort Deep throughout the Littorina Sea stage, together with Mn-Ca-P-carbonates. The formation of these P-bearing minerals in the Landsort Deep is likely controlled by a shelf-to-basin shuttle of Fe and Mn and high inputs of organic matter (including organic P) into the basin. We hypothesize that these P burial phases may also affect the P sequestration in other marine basins that experience a strong focusing of Fe and Mn.

Acknowledgements

This research was funded by the European Council under the European Community's Seventh Framework Programme (FP7/2007-2013)/ERC Starting Grant 278364 and the Netherlands Organisation for Scientific Research (NWO Vici Grant 865.13.005). This research used samples and data provided by the Integrated Ocean Drilling Program (IODP). We thank the captain and crew on board on the Greatship Manisha from 12th of September until and 1st of November 2013. P. Kraal is thanked for discussions and help at the ID21 beamline. We thank NWO and the European Synchrotron Facility for providing beamtime at ID21 and DUBBLE. We further acknowledge C. Rivard and D. Banerjee for their assistance at the beamlines and thank E. Smedberg for providing us with the Baltic Sea bathymetric map. The anonymous reviewers are gratefully acknowledged for their comments and suggestions.

References

Algeo, T.J., Ingall, E., 2007. Sedimentary Corg:P ratios, paleocean ventilation, and Phanerozoic atmospheric pO2. Palaeogeogr. Palaeoclimatol. Palaeoecol. 256, 130–155. doi:10.1016/j.palaeo.2007.02.029

Algeo, T.J., Lyons, T.W., 2006. Mo-total organic carbon covariation in modern anoxic marine environments: Implications for analysis of paleoredox and paleohydrographic conditions. Paleoceanography 21. doi:10.1029/2004PA001112

Anderson, M., Morel, F., 1982. The influence of aqueous iron chemistry on the uptake of iron by the coastal diatom Thalassiosira weissflogii1. Limnol. Oceanogr. 27, 789–813.

Anderson, T., Raiswell, R., 2004. Sources and mechanisms for the enrichment of highly reactive iron in euxinic Black Sea sediments. Am. J. Sci.

Andrén, E., Andrén, T., Sohlenius, G., 2000. The Holocene history of the southwestern Baltic Sea as reflected in a sediment core from the Bornholm Basin. Boreas 29, 233–250.

Andrén, T., Björck, S., Andrén, E., Conley, D., 2011. The development of the Baltic Sea Basin during the last 130 ka, in: Harff, J., Björck, S., Hoth, P. (Eds.), The Baltic Sea Basin. Springer-Verlag, Berlin, p. pp 75–97.

Andrén, T., Jørgensen, B.B., Cotterill, C., Green, S., Expedition 347 Scientists, 2015. Proc. IODP, 347. College Station, TX (Integrated Ocean Drilling Program).

Anschutz, P., Zhong, S., Sundby, B., Mucci, A., Gobeil, C., 1998. Burial efficiency of phosphorus and the geochemistry of iron in continental margin sediments. Limnol. Oceanogr. 43, 53–64. doi:10.4319/lo.1998.43.1.0053

APHA, 2005. Standard methods for the examination of water and wastewater. American Public Health Association – American Water Works Association – Water Environment Federation.

Berglund, B., Sandgren, P., Barnekow, L., 2005. Early Holocene history of the Baltic Sea, as reflected in coastal sediments in Blekinge, southeastern Sweden. Quat. Int. 130, 111–139.

Björck, S., 1995. A review of the history of the Baltic Sea, 13.0-8.0 ka BP. Quat. Int. 27, 19–40.

Borsboom, M., Bras, W., Cerjak, I., Detollenaere, D., Glastra van Loon, D., Goedtkindt, P., Konijnenburg, M., Lassing, P., Levine, Y.K., Munneke, B., Oversluizen, M., van Tol, R., Vlieg, E., 1998. The Dutch–Belgian beamline at the ESRF. J. Synchrotron Rad. 5, 518–520.

Böttcher, M.E., Lepland, A., 2000. Biogeochemistry of sulfur in a sediment core from the west-central Baltic Sea: Evidence from stable isotopes and pyrite textures. J. Mar. Syst. 25, 299–312. doi:10.1016/S0924-7963(00)00023-3

Burton, E.D., Sullivan, L. a., Bush, R.T., Johnston, S.G., Keene, A.F., 2008. A simple and inexpensive chromium-reducible sulfur method for acid-sulfate soils. Appl. Geochemistry 23, 2759–2766. doi:10.1016/j.apgeochem.2008.07.007

Canfield, D., Raiswell, R., Bottrell, S., 1992. The reactivity of sedimentary iron minerals toward sulfide. Am. J. Sci. 292, 659–683.

Canfield, D.E., 1994. Factors influencing organic carbon preservation in marine sediments. Chem. Geol. 114, 315–329. doi:10.1016/0009-2541(94)90061-2

Carman, R., Rahm, L., 1997. Early diagenesis and chemical characteristics of interstitial water and sediments in the deep deposition bottoms of the Baltic proper. J. Sea Res. 37, 25–47. doi:10.1016/S1385-1101(96)00003-2

Carstensen, J., Andersen, J.H., Gustafsson, B.G., Conley, D.J., 2014. Deoxygenation of the Baltic Sea during the last century. Proc. Natl. Acad. Sci. U. S. A. 111, 5628–33. doi:10.1073/pnas.1323156111

Casuccio, G.S., Schlaegle, S.F., Lersch, T.L., Huffman, G.P., Chen, Y., Shah, N., 2004. Measurement of fine particulate matter using electron microscopy techniques. Fuel Process. Technol. 85, 763–779. doi:10.1016/j.fuproc.2003.11.026

Conley, D.J., Björck, S., Bonsdorff, E., Carstensen, J., Destouni, G., Gustafsson, B.G., Hietanen, S., Kortekaas, M., Kuosa, H., Markus Meier, H.E., Müller-Karulis, B., Nordberg, K., Norkko, A., Nürnberg, G., Pitkänen, H., Rabalais, N.N., Rosenberg, R., Savchuk, O.P., Slomp, C.P., Voss, M., Wulff, F., Zillén, L., 2009. Hypoxia-Related Processes in the Baltic Sea. Environ. Sci. Technol. 43, 3412–3420. doi:10.1021/es802762a

Creveling, J.R., Johnston, D.T., Poulton, S.W., Kotrc, B., Marz, C., Schrag, D.P., Knoll, A.H., 2014. Phosphorus sources for phosphatic Cambrian carbonates. Geol. Soc. Am. Bull. 126, 145–163. doi:10.1130/B30819.1

De Lange, G.J., Thomson, J., Reitz, A., Slomp, C.P., Speranza Principato, M., Erba, E.,

Corselli, C., 2008. Synchronous basin-wide formation and redox-controlled preservation of a Mediterranean sapropel. Nat. Geosci. 1, 606–610. doi:10.1038/ngeo283

Dellwig, O., Leipe, T., März, C., Glockzin, M., Pollehne, F., Schnetger, B., Yakushev, E. V., Böttcher, M.E., Brumsack, H.-J., 2010. A new particulate Mn–Fe–P-shuttle at the redoxcline of anoxic basins. Geochim. Cosmochim. Acta 74, 7100–7115. doi:10.1016/j.gca.2010.09.017

Diaz, R.J., Rosenberg, R., 2008. Spreading dead zones and consequences for marine ecosystems. Science 321, 926–9. doi:10.1126/science.1156401

Dijkstra, N., Kraal, P., Kuypers, M.M.M., Schnetger, B., Slomp, C.P., 2014. Are iron-phosphate minerals a sink for phosphorus in anoxic Black Sea sediments? PLoS One 9, e101139. doi:10.1371/journal.pone.0101139

Drever, J., 1971. Magnesium-iron replacement in clay minerals in anoxic marine sediments. Science 172, 1334–1336.

Eckert, S., Brumsack, H.-J., Severmann, S., Schnetger, B., Marz, C., Frollje, H., 2013. Establishment of euxinic conditions in the Holocene Black Sea. Geology 41, 431–434. doi:10.1130/G33826.1

Egger, M., Jilbert, T., Behrends, T., Rivard, C., Slomp, C.P., 2015a. Vivianite is a major sink for phosphorus in methanogenic coastal surface sediments. Geochim. Cosmochim. Acta 169, 217–235. doi:10.1016/j.gca.2015.09.012

Egger, M., Rasigraf, O., Sapart, C.J., Jilbert, T., Jetten, M.S.M., Röckmann, T., Van Der Veen, C., Banda, N., Kartal, B., Ettwig, K.F., Slomp, C.P., 2015b. Iron-mediated anaerobic oxidation of methane in brackish coastal sediments. Environ. Sci. Technol. 49, 277–283. doi:10.1021/es503663z

Emelyanov, E.M., 2001. Biogenic components and elements in sediments of the Central Baltic and their redistribution. Mar. Geol. 172, 23–41. doi:10.1016/S0025-3227(00)00121-3

Erickson, B.E., Helz, G.R., 2000. Molybdenum(VI) speciation in sulfidic waters: Geochim. Cosmochim. Acta 64, 1149–1158. doi:10.1016/S0016-7037(99)00423-8

Faul, K.L., Paytan, A., Delaney, M.L., 2005. Phosphorus distribution in sinking oceanic particulate matter. Mar. Chem. 97, 307–333. doi:10.1016/j.marchem.2005.04.002

Fehr, M. a., Andersson, P.S., Hålenius, U., Mörth, C.-M., 2008. Iron isotope variations in Holocene sediments of the Gotland Deep, Baltic Sea. Geochim. Cosmochim. Acta 72, 807–826. doi:10.1016/j.gca.2007.11.033

Fonselius, S., 1981. Oxygen and hydrogen sulphide conditions in the Baltic Sea. Mar. Pollut. Bull. 12, 187–194.

Froelich, P., Bender, M., Luedtke, N., 1982. The marine phosphorus cycle. Am. J. Sci. 282, 474–511.

Funkey, C.P., Conley, D.J., Reuss, N.S., Humborg, C., Jilbert, T., Slomp, C.P., 2014. Hypoxia sustains cyanobacteria blooms in the baltic sea. Environ. Sci. Technol. 48, 2598–602. doi:10.1021/es404395a

Gächter, R., Meyer, J.S., Mares, A., 1988. Contribution of bacteria to release and fixation of phosphorus in lake sediments. Limnol. Oceanogr. 33, 1542–1558. doi:10.4319/lo.1988.33.6part2.1542

Ganeshram, R.S., Pedersen, T.F., Calvert, S., François, R., 2002. Reduced nitrogen fixation in the glacial ocean inferred from changes in marine nitrogen and phosphorus inventories. Nature 415, 156–9. doi:10.1038/415156a

Grasshoff, K., Ehrhardt, M., Kremling, K., 1983. No Title, in: Methods of Seawater Analysis (2nd Edn). p. 417.

Gustafsson, B., Schenk, F., Blenckner, T., Eilola, K., Meier, H.E.M., Müller-Karulis, B., Neumann, T., Ruoho-Airola, T., Savchuk, O.P., Zorita, E., 2012. Reconstructing the development of Baltic Sea eutrophication 1850–2006. Ambio 41, 534–548.

Hall, P.O.J., Aller, R.C., 1992. Rapid, small-volume, flow injection analysis for SCO2, and NH4+ in marine and freshwaters. Limnol. Oceanogr. 37, 1113–1119. doi:10.4319/lo.1992.37.5.1113

Hartnett, H.E., Keil, R.G., Hedges, J.I., Devol, A.H., 1998. Influence of oxygen exposure time on organic carbon preservation in continental margin sediments 391, 572–575. doi:10.1038/35351

Holmkvist, L., Kamyshny, A., Vogt, C., Vamvakopoulos, K., Ferdelman, T.G., Jørgensen, B.B., 2011. Sulfate reduction below the sulfate–methane transition in Black Sea sediments. Deep Sea Res. Part I Oceanogr. Res. Pap. 58, 493–504. doi:10.1016/j.dsr.2011.02.009

Hsu, T., Jiang, W., Wang, Y., 2014. Authigenesis of vivianite as influenced by methane-induced sulfidization in cold-seep sediments off southwestern Taiwan. J. Asian Earth Sci. 89, 88–97.

Huckriede, H., Meischner, D., 1996. Origin and environment of manganese-rich sediments within black-shale basins. Geochim. Cosmochim. Acta 60, 1399–1413. doi:10.1016/0016-7037(96)00008-7

Ingall, E., Jahnke, R., 1994. Evidence for enhanced phosphorus regeneration from marine sediments overlain by oxygen depleted waters. Geochim. Cosmochim. Acta 58, 2571–2575. doi:10.1016/0016-7037(94)90033-7

Ingall, E.D., Bustin, R.M., Van Cappellen, P., 1993. Influence of water column anoxia on the burial and preservation of carbon and phosphorus in marine shales. Geochim. Cosmochim. Acta 57, 303–316. doi:10.1016/0016-7037(93)90433-W

Ingall, E.D., Jahnke, R., 1997. Influence of water-column anoxia on the elemental fractionation of carbon and phosphorus during sediment diagenesis. Mar. Geol. 139, 219–229. doi:10.1016/S0025-3227(96)00112-0

Jahnke, R., 1984. The synthesis and solubility of carbonate fluorapatite. Am. J. Sci. 284, 58–78.

Jakobsen, R., Postma, D., 1989. Formation and solid solution behavior of Ca-rhodochrosites in marine muds of the Baltic deeps. Geochim. Cosmochim. Acta 53, 2639–2648. doi:10.1016/0016-7037(89)90135-X

Jensen, H., McGlathery, K., Marino, R., Howarth, R.W., 1998. Forms and availability of sediment phosphorus in carbonate sand of Bermuda seagrass beds. Limnol. Oceanogr. 43, 799–810.

Jilbert, T., Slomp, C.P., 2013a. Iron and manganese shuttles control the formation of authigenic phosphorus minerals in the euxinic basins of the Baltic Sea. Geochim. Cosmochim. Acta 107, 155–169. doi:10.1016/j.gca.2013.01.005

Jilbert, T., Slomp, C.P., 2013b. Rapid high-amplitude variability in Baltic Sea hypoxia during the Holocene. Geology 41, 1183–1186. doi:10.1130/G34804.1

Jilbert, T., Slomp, C.P., Gustafsson, B.G., Boer, W., 2011. Beyond the Fe-P-redox connection: preferential regeneration of phosphorus from organic matter as a key control on Baltic Sea nutrient cycles. Biogeosciences 8, 1699–1720. doi:10.5194/bg-8-1699-2011

Katsikopoulos, D., Fernández-González, Á., Prieto, M., 2009. Precipitation and mixing properties of the "disordered" (Mn,Ca)CO3 solid solution. Geochim. Cosmochim. Acta 73, 6147–6161. doi:10.1016/j.gca.2009.07.001

Kraal, P., Slomp, C.P., 2014. Rapid and Extensive Alteration of Phosphorus Speciation during Oxic Storage of Wet Sediment Samples. PLoS One 9, e96859. doi:10.1371/journal.pone.0096859

Kraal, P., Slomp, C.P., Forster, A., Kuypers, M.M.M., Sluijs, A., 2009. Pyrite oxidation during sample storage determines phosphorus fractionation in carbonate-poor anoxic sediments. Geochim. Cosmochim. Acta 73, 3277–3290. doi:10.1016/j.gca.2009.02.026

Lenz, C., Behrends, T., Jilbert, T., Silveira, M., Slomp, C.P., 2014. Redox-dependent changes in manganese speciation in Baltic Sea sediments from the Holocene Thermal Maximum: An EXAFS, XANES and LA-ICP-MS study. Chem. Geol. 370, 49–57. doi:10.1016/j.chemgeo.2014.01.013

Lenz, C., Jilbert, T., Conley, D.J., Wolthers, M., Slomp, C.P., 2015. Are recent changes in sediment manganese sequestration in the euxinic basins of the Baltic Sea linked to the expansion of hypoxia? Biogeosciences 12, 4875–4894. doi:10.5194/bg-12-4875-2015

Lepland, A., Stevens, R.L., 1998. Manganese authigenesis in the Landsort Deep , Baltic Sea. Mar. Geol. 151, 1–25.

Lewis, B.L., Landing, W.M., 1991. The biogeochemistry of manganese and iron in the Black Sea. Deep Sea Res. Part A. Oceanogr. Res. Pap. 38, S773–S803. doi:10.1016/S0198-0149(10)80009-3

Li, W., Joshi, S.R., Hou, G., Burdige, D.J., Sparks, D.L., Jaisi, D.P., 2015. Characterizing phosphorus speciation of Chesapeake Bay sediments using chemical extraction, 31P NMR, and X-ray absorption fine structure spectroscopy. Environ. Sci. Technol. 49, 203–11. doi:10.1021/es504648d

Loh, A.N., Bauer, J.E., 2000. Distribution, partitioning and fluxes of dissolved and particulate organic C, N and P in the eastern North Pacific and Southern Oceans. Deep Sea Res. Part I Oceanogr. Res. Pap. 47, 2287–2316. doi:10.1016/S0967-0637(00)00027-3

Lyons, T.W., Severmann, S., 2006. A critical look at iron paleoredox proxies: New insights from modern euxinic marine basins. Geochim. Cosmochim. Acta 70, 5698–5722. doi:10.1016/j.gca.2006.08.021

Manceau, A., Marcus, M.A., Grangeon, S., 2012. Determination of Mn valence states in mixed-valent manganates by XANES spectroscopy. Am. Mineral. 97, 816–827. doi:10.2138/am.2012.3903

Matthäus, W., Nausch, G., 2003. Hydrographic-hydrochemical variability in the Baltic Sea during the 1990s in relation to changes during the 20th century. ICES Mar. Sci.

Symp. 219, 132–143.

Middelburg, J.J., de Lange, G.J., van der Weijden, C.H., 1987. Manganese solubility control in marine pore waters. Geochemica Cosmochim. Acta 51, 759–763.

Moodley, L., Middelburg, J.J., Herman, P.M.J., Soetaert, K., de Lange, G.J., 2005. Oxygenation and organic-matter preservation in marine sediments: Direct experimental evidence from ancient organic carbon–rich deposits. Geology 33, 889. doi:10.1130/G21731.1

Mort, H.P., Slomp, C.P., Gustafsson, B.G., Andersen, T.J., 2010. Phosphorus recycling and burial in Baltic Sea sediments with contrasting redox conditions. Geochim. Cosmochim. Acta 74, 1350–1362. doi:10.1016/j.gca.2009.11.016

Mortimer, C., 1941. The exchange of dissolved substances between mud and water in lakes. J. Ecol. 29, 280–329.

Murphy, T., Lawson, A., Kumagai, M., Nalewajko, C., 2001. Release of phosphorus from sediments in Lake Biwa. Limnology 2, 119–128. doi:10.1007/s102010170007

Nakano, S., 1992. Manganoan vivianite in the bottom sediments of Lake Biwa, Japan. Mineral. J. 16, 96–107. doi:10.2465/minerj.16.96

Nembrini, G.P., Capobianco, J.A., Viel, M., Williams, A.F., 1983. A Mössbauer and chemical study of the formation of vivianite in sediments of Lago Maggiore (Italy). Geochim. Cosmochim. Acta 47, 1459–1464. doi:10.1016/0016-7037(83)90304-6

Nikitenko, S., Beale, A., van der Eerden, A.M.J., Jacques, S.D.M., Leynaud, O., O'Brien, M.G., Detollenaere, D., Kaptein, R., Weckhuysen, B.M., Bras, W., 2008. Implementation of a combined SAXS/WAXS/QEXAFS set-up for time-resolved in situ experiments. J. Synchrotron Radiat. 15, 632–640.

Nriagu, J.O., 1972. Stability of vivianite and ion-pair formation in the system fe3(PO4)2-H3PO4H3PO4-H2o. Geochim. Cosmochim. Acta 36, 459–470. doi:10.1016/0016-7037(72)90035-X

O'Connell, D.W., Mark Jensen, M., Jakobsen, R., Thamdrup, B., Joest Andersen, T., Kovacs, A., Bruun Hansen, H.C., 2015. Vivianite formation and its role in phosphorus retention in Lake Ørn, Denmark. Chem. Geol. 409, 42–53. doi:10.1016/j.chemgeo.2015.05.002

Poulton, S., Canfield, D., 2005. Development of a sequential extraction procedure for iron: implications for iron partitioning in continentally derived particulates. Chem. Geol. 214, 209–221. doi:10.1016/j.chemgeo.2004.09.003

Raiswell, R., Anderson, T.F., 2005. Reactive iron enrichment in sediments deposited beneath euxinic bottom waters: constraints on supply by shelf recycling. Geol. Soc. London, Spec. Publ. 248, 179–194. doi:10.1144/GSL.SP.2005.248.01.10

Raiswell, R., Canfield, D.E., 2012. The Iron Biogeochemical Cycle Past and Present. Geochem. Perspect 1, 1–232.

Ravel, B., Newville, M., 2005. ATHENA, ARTEMIS, HEPHAESTUS: data analysis for X-ray absorption spectroscopy using IFEFFIT. J. Synchrotron Radiat. 12, 537–41. doi:10.1107/S0909049505012719

Reed, D.C., Gustafsson, B.G., Slomp, C.P., 2015. Shelf-to-basin iron shuttling enhances vivianite formation in deep Baltic Sea sediments. Earth Planet. Sci. Lett. 1, 1–11. doi:10.1016/j.epsl.2015.11.033

Reed, D.C., Slomp, C.P., de Lange, G.J., 2011a. A quantitative reconstruction of organic matter and nutrient diagenesis in Mediterranean Sea sediments over the Holocene. Geochim. Cosmochim. Acta 75, 5540–5558. doi:10.1016/j.gca.2011.07.002

Reed, D.C., Slomp, C.P., Gustafsson, B.G., 2011b. Sedimentary phosphorus dynamics and the evolution of bottom-water hypoxia: A coupled benthic-pelagic model of a coastal system. Limnol. Oceanogr. 56, 1075–1092. doi:10.4319/lo.2011.56.3.1075

Rothe, M., Kleeberg, A., Grüneberg, B., Friese, K., Pérez-Mayo, M., Hupfer, M., 2015. Sedimentary Sulphur:Iron Ratio Indicates Vivianite Occurrence: A Study from Two Contrasting Freshwater Systems. PLoS One 10, e0143737. doi:10.1371/journal.pone.0143737

Rothe, M., Kleeberg, A., Hupfer, M., 2016. The occurrence, identification and environmental relevance of vivianite in waterlogged soils and aquatic sediments. Earth-Science Rev. 158, 51–64. doi:10.1016/j.earscirev.2016.04.008

Rouzies, D., Millet, J.M.M., Lyon, I., Einstein, A., Cedex, F.V., 1993. Mossbauer study of synthetic oxidized vivianite at room temperature. Hyperfine Interact. 77, 19–28.

Rutten, A., de Lange, G.J., 2003. Sequential extraction of iron, manganese and related elements in S1 sapropel sediments, eastern Mediterranean. Palaeogeogr. Palaeoclimatol. Palaeoecol. 190, 79–101. doi:10.1016/S0031-0182(02)00600-4

Ruttenberg, K.C., 1992. Development of a sequential extraction method for different forms of phosphorus in marine sediments. Limnol. Oceanogr. 37, 1460–1482.

Ruttenberg, K.C., 2003. The global phosphorus cycle, in: Treatise on Geochemistry 8. pp. 585–643.

Ruttenberg, K.C., Berner, R.A., 1993. Authigenic apatite formation and burial in sediments from non-upwelling, continental margin environments. Geochim. Cosmochim. Acta 57, 991–1007. doi:10.1016/0016-7037(93)90035-U

Salomé, M., Cotte, M., Baker, R., Barrett, R., Benseny-Cases, N., Berruyer, G., Bugnazet, D., Castillo-Michel, H., Cornu, C., Fayard, B., Gagliardini, E., Hino, R., Morse, J., Papillon, E., Pouyet, E., Rivard, C., Solé, V.A., Susini, J., Veronesi, G., 2013. The ID21 Scanning X-ray Microscope at ESRF. J. Phys. Conf. Ser. 425, 182004. doi:10.1088/1742-6596/425/18/182004

Santvoort, P.J.M. Van, Lange, G.J. De, Thomson, J., Colley, S., Meysman, F.J.R., Slomp, C.P., 2002. Oxidation and Origin of Organic Matter in Surficial Eastern Mediterranean Hemipelagic Sediments. Aquat. Geochemistry 8, 153–175. doi:10.1023/A:1024271706896

Sapota, T., Aldahan, A., Al-Aasm, I.S., 2006. Sedimentary facies and climate control on formation of vivianite and siderite microconcretions in sediments of Lake Baikal, Siberia. J. Paleolimnol. 36, 245–257. doi:10.1007/s10933-006-9005-x

Schenau, S.J., De Lange, G.J., 2000. A novel chemical method to quantify fish debris in marine sediments. Limnol. Oceanogr. 45, 963–971. doi:10.4319/lo.2000.45.4.0963

Scholz, F., McManus, J., Sommer, S., 2013. The manganese and iron shuttle in a modern euxinic basin and implications for molybdenum cycling at euxinic ocean margins. Chem. Geol. 355, 56–68.

Scholz, F., Severmann, S., 2014. Beyond the Black Sea paradigm: The sedimentary fingerprint of an open-marine iron shuttle. Geochemica Cosmochim. Acta 127, 368–

380.

Slomp, C.P., Epping, E.H.G., Helder, W., Raaphorst, W. Van, 1996. A key role for iron-bound phosphorus in authigenic apatite formation in North Atlantic continental platform sediments. J. Mar. Res. 54, 1179–1205. doi:10.1357/0022240963213745

Slomp, C.P., Mort, H.P., Jilbert, T., Reed, D.C., Gustafsson, B.G., Wolthers, M., 2013. Coupled dynamics of iron and phosphorus in sediments of an oligotrophic coastal basin and the impact of anaerobic oxidation of methane. PLoS One 8, e62386. doi:10.1371/journal.pone.0062386

Slomp, C.P., Van Cappellen, P., 2007. The global marine phosphorus cycle: sensitivity to oceanic circulation. Biogeosciences 4, 155–171. doi:10.5194/bg-4-155-2007

Sohlenius, G., Emeis, K., Andrén, E., Andrén, T., Kohly, A., 2001. Development of anoxia during the Holocene fresh–brackish water transition in the Baltic Sea. Mar. Geol. 177, 221–242.

Steenbergh, A.K., Bodelier, P.L.E., Heldal, M., Slomp, C.P., Laanbroek, H.J., 2013. Does microbial stoichiometry modulate eutrophication of aquatic ecosystems? Environ. Microbiol. 15, 1572–9. doi:10.1111/1462-2920.12042

Steenbergh, A.K., Bodelier, P.L.E., Hoogveld, H.L., Slomp, C.P., Laanbroek, H.J., 2011. Phosphatases relieve carbon limitation of microbial activity in Baltic Sea sediments along a redox-gradient. Limnol. Oceanogr. 56, 2018–2026. doi:10.4319/lo.2011.56.6.2018

Stipp, S., Hochella, M., Parks, G., Leckie, J., 1992. Cd2+ uptake by calcite, solid-state diffusion, and the formation of solid-solution: Interface processes observed with near-surface sensitive techniques (XPS, LEED, and AES). Geochemica Cosmochim. Acta 56, 1941–1954.

Strickland, T.D.H., Parsons, T.R., 1972. A Practical Handbook of Seawater Analysis.

Suess, E., 1979. Mineral phases formed in anoxic sediments by microbial decomposition of organic matter. Geochim. Cosmochim. Acta 43, 339–352. doi:10.1016/0016-7037(79)90199-6

Thibault, P.-J., Rancourt, D.G., Evans, R.J., Dutrizac, J.E., 2009. Mineralogical confirmation of a near-P:Fe=1:2 limiting stoichiometric ratio in colloidal P-bearing ferrihydrite-like hydrous ferric oxide. Geochim. Cosmochim. Acta 73, 364–376. doi:10.1016/j.gca.2008.10.031

Tsandev, I., Reed, D.C., Slomp, C.P., 2012. Phosphorus diagenesis in deep-sea sediments: Sensitivity to water column conditions and global scale implications. Chem. Geol. 330-331, 127–139. doi:10.1016/j.chemgeo.2012.08.012

Tyrrell, T., 1999. The relative influences of nitrogen and phosphorus on oceanic primary production. Nature 400, 525–531. doi:10.1038/22941

Van Cappellen, P., Ingall, E.D., 1994. Benthic phosphorus regeneration , net primary production , and ocean anoxia : A model of the coupled marine biogeochemical cycles of carbon and phosphorus. Palaeogeography 9, 677–692.

von Breymann, M.T., Collier, R., Suess, E., 1990. Magnesium adsorption and ion exchange in marine sediments: A multi-component model. Geochim. Cosmochim. Acta 54, 3295–3313. doi:10.1016/0016-7037(90)90286-T

Wallmann, K., Aloisi, G., Haeckel, M., Tishchenko, P., Pavlova, G., Greinert, J., Kutterolf, S.,

Eisenhauer, A., 2008. Silicate weathering in anoxic marine sediments. Geochim. Cosmochim. Acta 72, 2895–2918. doi:10.1016/j.gca.2008.03.026

Wijsman, J., Middelburg, J., Heip, C., 2001. Reactive iron in Black Sea sediments: implications for iron cycling. Mar. Geol. 172, 167–180.

Yakubovich, O. V., Massa, W., Liferovich, R.P., McCammon, C.A., 2001. The crystal structure of baricite (Mg1.70Fe1.30)(PO4)2.8H2O, the magnesium-dominant member of the vivianite group. Can. Mineral. 39, 1317–1324. doi:10.2113/gscanmin.39.5.1317

Zelibor, J., Senftle, F., Reinhardt, J., 1988. A proposed mechanism for the formation of spherical vivianite crystal aggregates in sediments. Sediment. Geol. 59, 125–142.

Zillén, L., Conley, D.J., Andrén, T., Andrén, E., Björck, S., 2008. Past occurrences of hypoxia in the Baltic Sea and the role of climate variability, environmental change and human impact. Earth-Science Rev. 91, 77–92. doi:10.1016/j.earscirev.2008.10.001

Figure and table captions

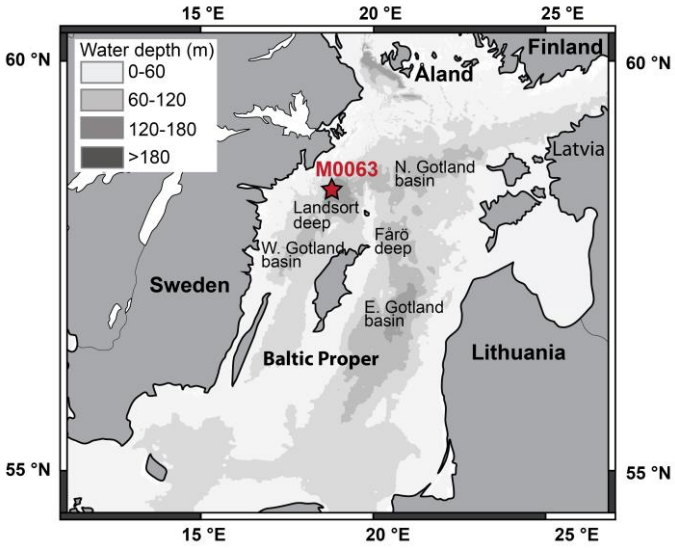

Fig. 1: Bathymetric map of the Baltic Proper with its key basins. Our study site (M0063) is located in the Landsort Deep, the deepest basin of the Baltic Sea.

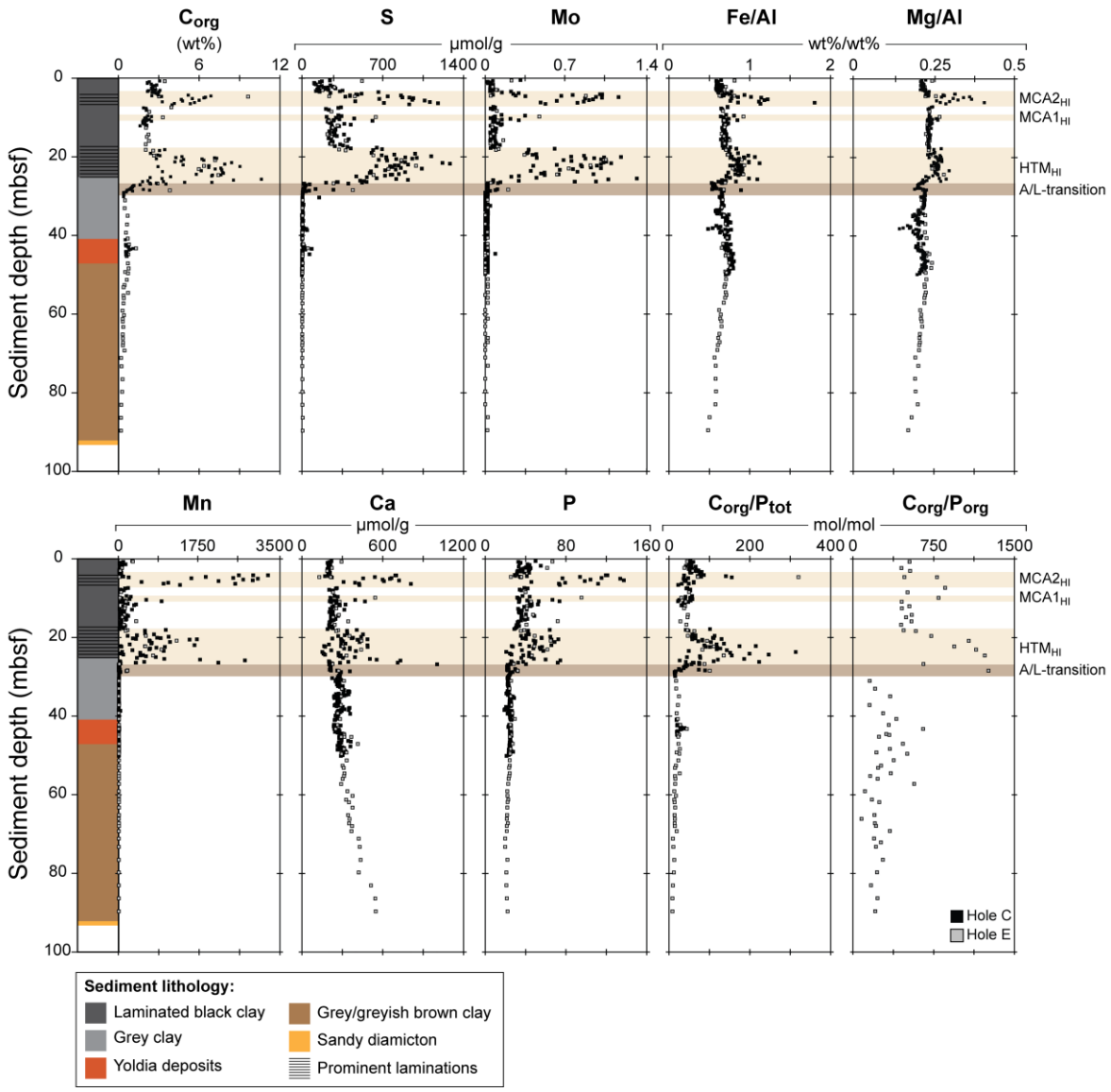

Fig. 2: Sediment profiles of C_{org} (organic C), total S, Mo, Fe/Al, Mg/Al, Mn, Ca, P and C_{org}/P_{tot} and C_{org}/P_{org}. The sediment lithology is a simplified version of the core description for Hole C, see section 2.1 and (Andrén et al., 2015). The A/L transition defines the transition from the Ancyclus Lake to the Littorina Sea within the sediment record. Hypoxic intervals are highlighted by light brown bars (HTM_{HI}, $MCA1_{HI}$ and $MCA2_{HI}$).

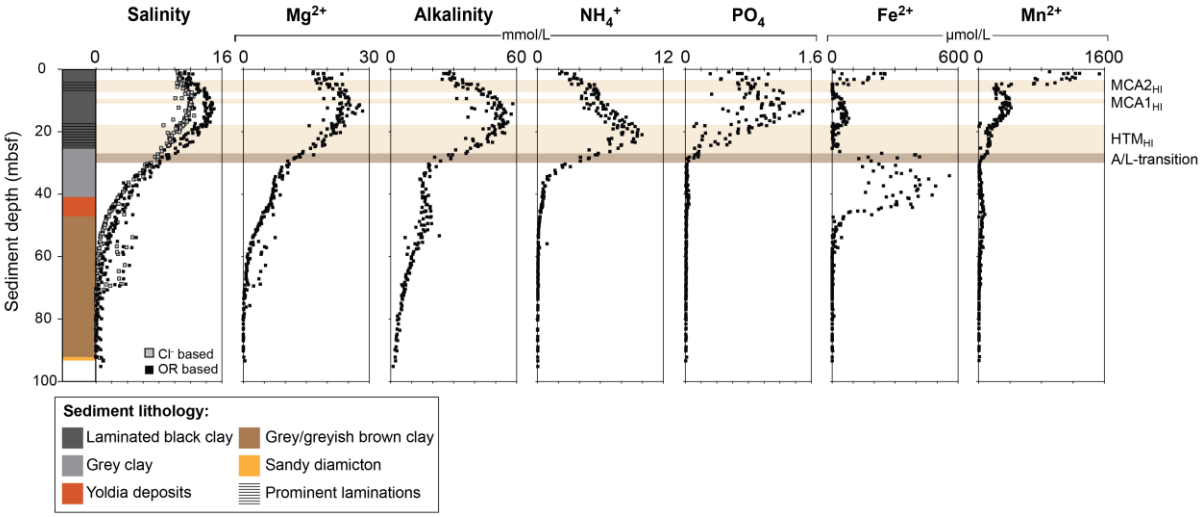

Fig. 3: Porewater depth profiles for salinity, magnesium (Mg^{2+}), alkalinity, ammonium (NH_4^+), phosphate (PO_4), iron (Fe^{2+}) and manganese (Mn^{2+}). Sediment lithology: see caption of Fig. 2. Porewater samples from all holes (A-E) are shown. Both the salinity as calculated based on the Cl^- contents in the porewater (Cl^- based) and as measured with an optical refractor (OR based) is shown. We did not differentiate between the different holes (A-E) as major trends in porewater were similar for the different holes.

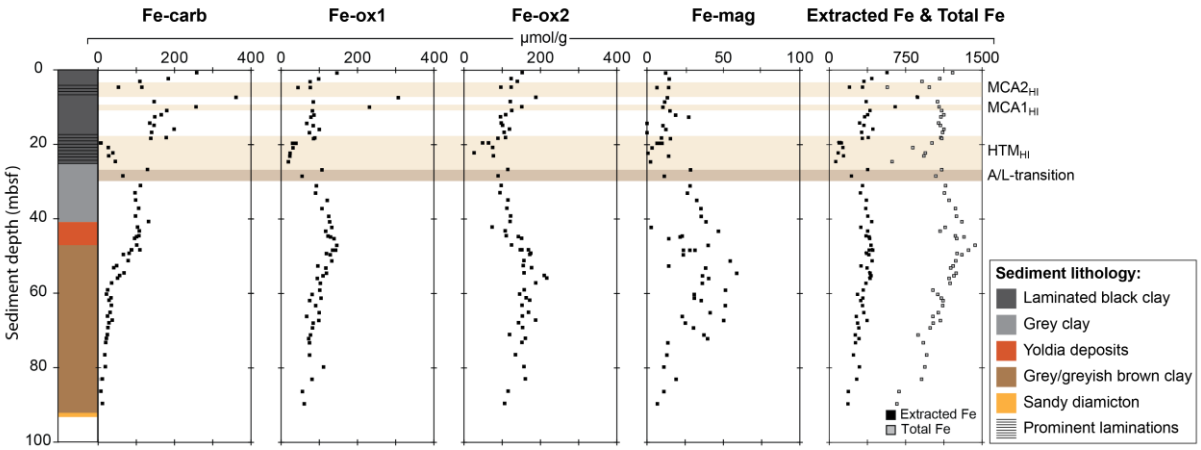

Fig. 4: Depth profiles of solid phase iron fractions for Hole E. Sediment lithology: see caption of Fig. 2. The fractions are Fe-carbonates (Fe-carb), amorphous Fe-oxides (Fe-ox1), crystalline Fe-oxides and magnetite (Fe-mag). On average, the sum of these Fe-fractions accounts for ~ 30% of the total Fe pool in the sediments.

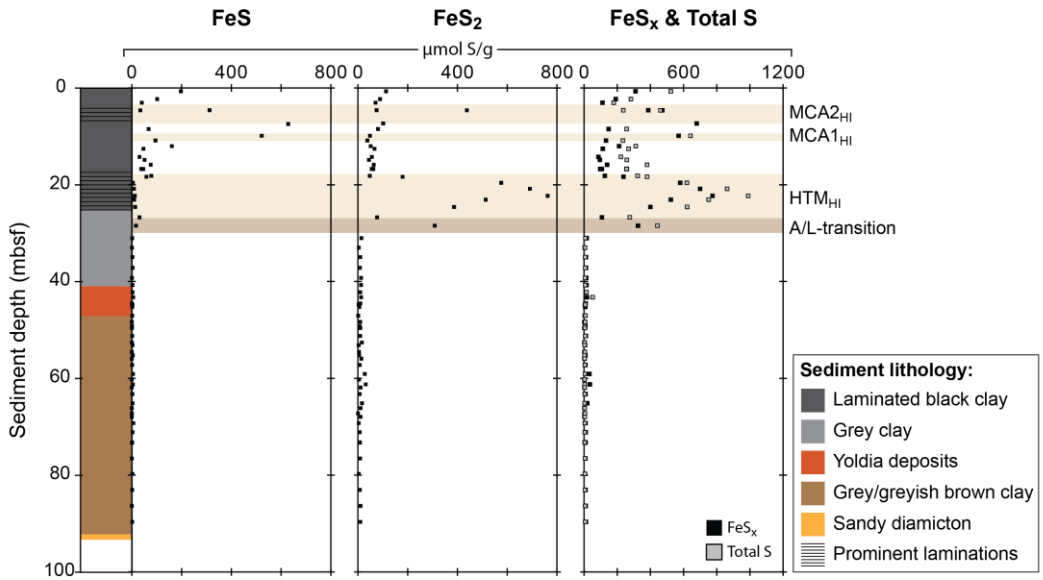

Fig. 5: Depth profiles of solid sulfur fractions for Hole E. Sediment lithology: see caption of Fig. 2. The S phases, as determined by the method of Burton et al. (2008), are iron monosulfides (FeS) and pyrite (FeS_2). In the upper 30 m of the sediments, the extracted sulfur phases (FeS_x) account for ~ 70 % of the total S pool.

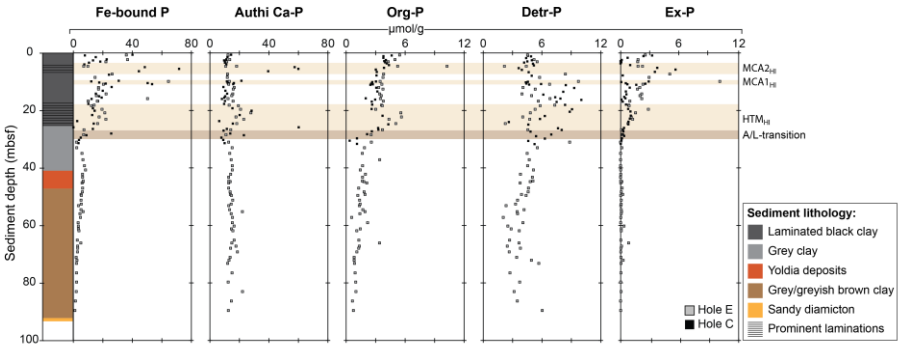

Fig. 6: Depth profiles of phosphorus phases for Hole E and C. Sediment lithology: see caption of Fig. 2. The phases are Fe-bound P, authigenic Ca-P (Authi Ca-P), organic P (Org-P), detrital P (Detr-P) and exchangeable P (Ex-P).

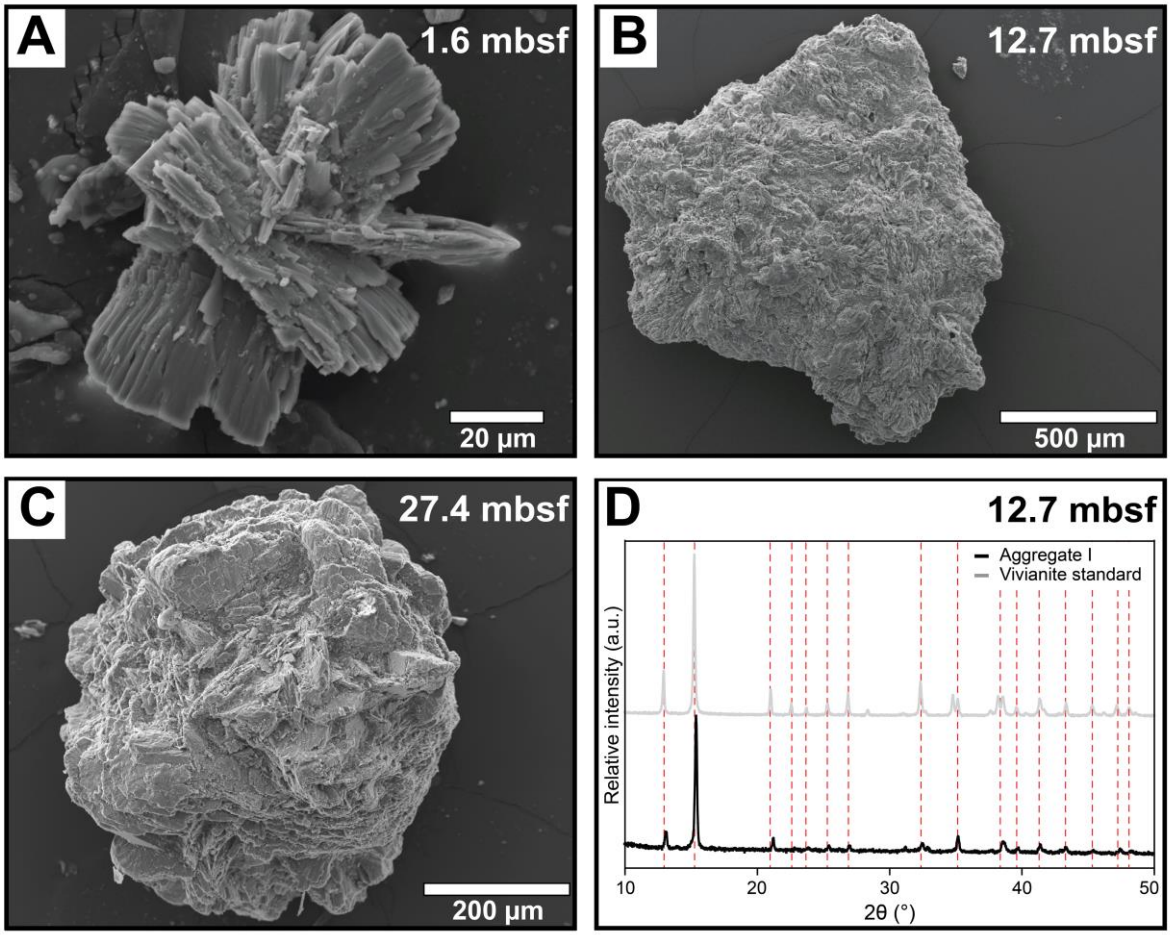

Fig. 7: Morphology and chemical analysis of the sieved aggregates as determined with SEM (A-C) and XRD (D). Aggregates from three depths were examined with the SEM in scanning electron mode. The morphology ranged from small platy- and needle-shaped crystals (A) to larger less crystalline aggregates (B) and spherical aggregates (C). All depths are given in meters below seafloor (mbsf). Please note the differences in scales. XRD analysis was conducted on an aggregate from 12.7 mbsf (Aggregate I) and its spectrum shows large similarities with the XRD spectrum for our in-house synthesized vivianite standard (D; dotted red lines mark peaks at similar angles).

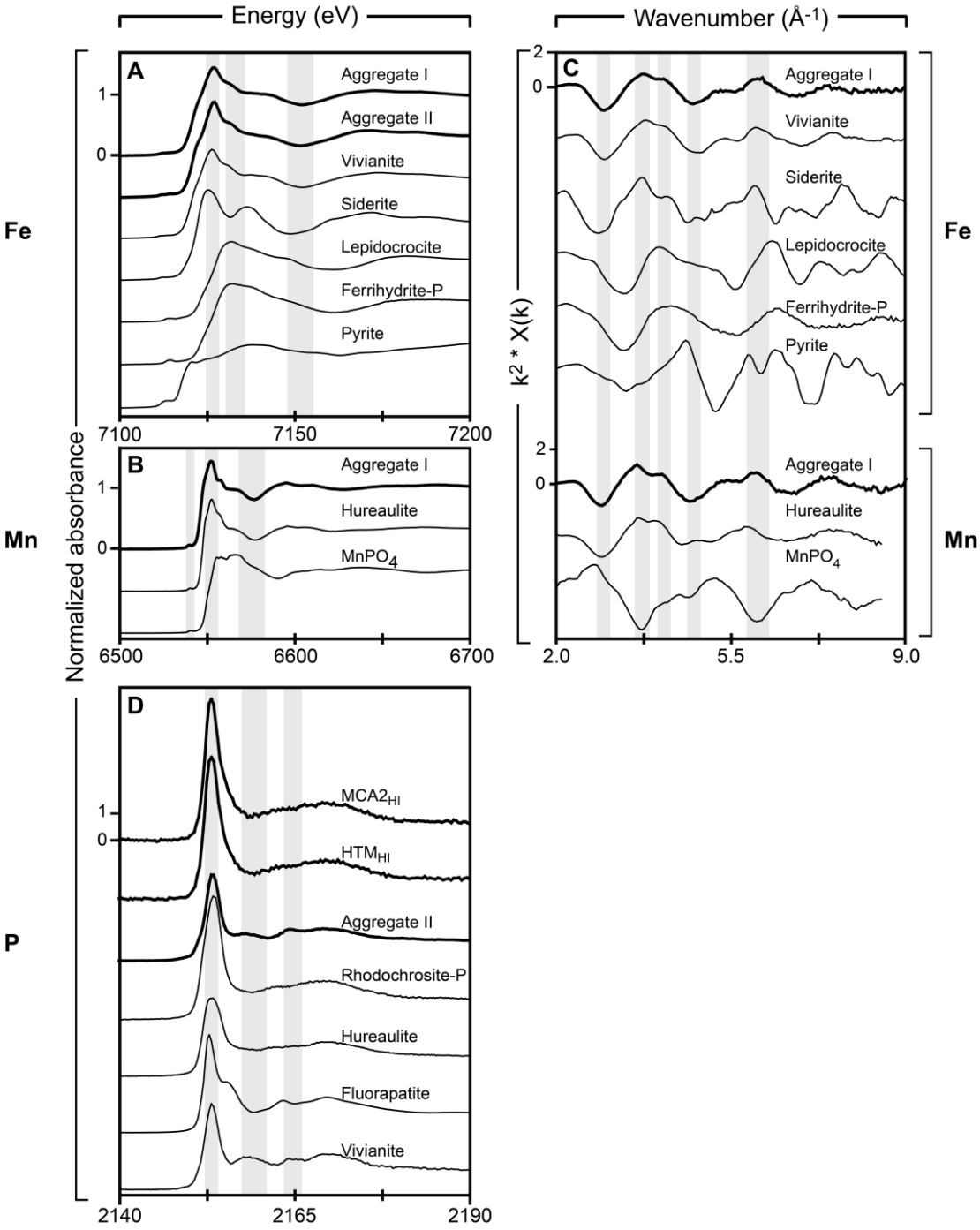

Fig. 8: EXAFS and normalized XANES spectra of bulk sediments from the HTM_{HI} (20.83 m) and the $MCA2_{HI}$ (7.34 m), individual aggregates from 12.7 m depth (I and II) and reference materials. Fe XANES spectra (A), Mn XANES spectra (B), Fe and Mn EXAFS (C) and (D) P XANES spectra. The reference materials are described in Table 2.

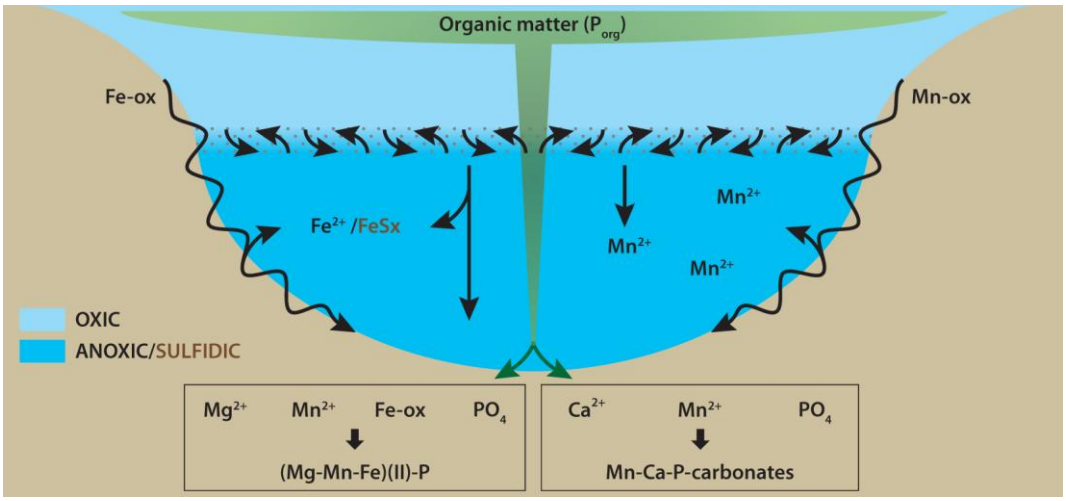

Fig. 9: A schematic of the coupling between the Fe and Mn shelf-to-basin shuttle, primary productivity and P burial at Landsort Deep. The surface waters are highly productive, which results in a flux of organic matter (including organic P (P_{org})) towards the seafloor. In the anoxic or sulfidic surface sediments, PO_4 is released by organic matter decomposition. At the same time, Fe-oxides (Fe-ox) are shuttled into the basin via multiple cycles of re-oxidation, deposition and re-mobilization. Some Fe may also be transported through the redoxcline. The portion of Fe-oxides that dissolves in the deep basin to Fe^{2+} and is converted to FeS_x depends on the balance between S availability in the water column and the input of Fe-oxides into the basin. Also Mn-oxides (Mn-ox) are shuttled into the anoxic or sulfidic basin and are partly reduced in the anoxic or sulfidic water column with Mn being released as Mn^{2+}. Together with sufficient porewater Mg^{2+} and Ca^{2+}, these circumstances promote the formation of vivianite rich in Mn and Mg ((Mg-Mn-Fe)(II)-P) and Mn-Ca-P-carbonates in the near-surface sediments in the anoxic or sulfidic deep basin.

Table 1: Reference samples used for XANES and EXAFS spectroscopy.

	Name	Formula	Description and/or source
Fe	Vivianite	$(Fe^{2+})_3(PO_4)_2.8H_2O$	Egger et al. (2015)
	Siderite	$FeCO_3$	Purchased from Ward's Natural Science. Mine location: Queenstown, Quebec, Canada
	Lepidocrosite	γ-FeO(OH)	Purchased from Lanxess (Leverkusen, German). Trade name: Bayferrox 943
	ferrihydrite with co-precipitated PO_4	Hydrated $Fe^{3+}{}_{10}O_{14}(OH)_2(PO_4)$	Egger et al. (2015)
	Pyrite	FeS_2	Purchased from Ward's Natural Science. Mine location: Zacatecas, Mexico
Mn	Hureaulite	$(Mn^{2+})_5(PO_4)[PO_3(OH)]_2.4H_2O$	Manceau et al. (2012)
	MnPO4	$(Mn^{3+})(PO_4)$	Manceau et al. (2012)
P	Vivianite	$(Fe^{2+})_3(PO_4)_2.8H_2O$	Egger et al. (2015)
	Carbonate fluorapatite	$Ca_5(PO_4, CO_3)_3 F$	Synthesized as described by Jahnke (1984)
	Hureaulite	$(Mn^{2+})_5(PO_4)[PO_3(OH)]_2.4H_2O$	Egger et al. (2015)
	Rhodochrosite with co-precipitated PO_4	$(Mn^{2+})CO_3(PO_4)$	Synthesized as described by Katsikopoulos et al. (2009) and precipitated in the presence of 1M PO_4

Table 2: Relative elemental abundances in mol% and molar ratios in mol/mol in a whole aggregate (12.7 mbsf) and for surfaces of multiple aggregates (1.6, 12.7 and 27.4 mbsf). The molar ratios for the whole aggregate were determined by total destruction and ICP-OES, while the elemental distribution and ratios for the aggregate surfaces were estimated with SEM-EDS (n=number of measurements). Different superscripts indicate statistical differences in means between the groups (one-way ANOVA tests; $p<0.05$). P-values for all statistical differences were <0.005, except for Si ($p = 0.034$).

	Whole aggregate	**Aggregate surface**					
	12.7 m (n=1)	1.6 m (n=9)		12.7 m (n=9)		27.4 m (n=11)	
	MEAN	MEAN	*ST. DEV*	MEAN	*ST. DEV*	MEAN	*ST. DEV*
P	37	16[a]	*12*	14[a]	*10*	6[a]	*7*
Fe	21	51[a]	*13*	21[b]	*6*	64[a]	*26*
Mn	17	28[a]	*11*	11[b]	*11*	7[b]	*3*
Mg	21	3[a]	*4*	20[b]	*11*	2[a]	*3*
Si	-	2[a]	*2*	28[b]	*26*	15[a-b]	*25*
Al	4.0	1[a]	1	6[a]	5	6[a]	7
Fe/P	0.58	3.2		1.5		10.3	
Mn/P	0.56	1.8		0.8		1.1	
Mg/P	0.47	0.2		1.4		0.4	
(Fe,Mn,Mg)/P	1.6	5.2		3.7		11.8	

Supplementary information

Vivianite is a key sink for phosphorus in sediments of the Landsort Deep, an intermittently anoxic deep basin in the Baltic Sea

S1: Organic carbon content (C_{org}) versus Mo for several brackish/marine systems

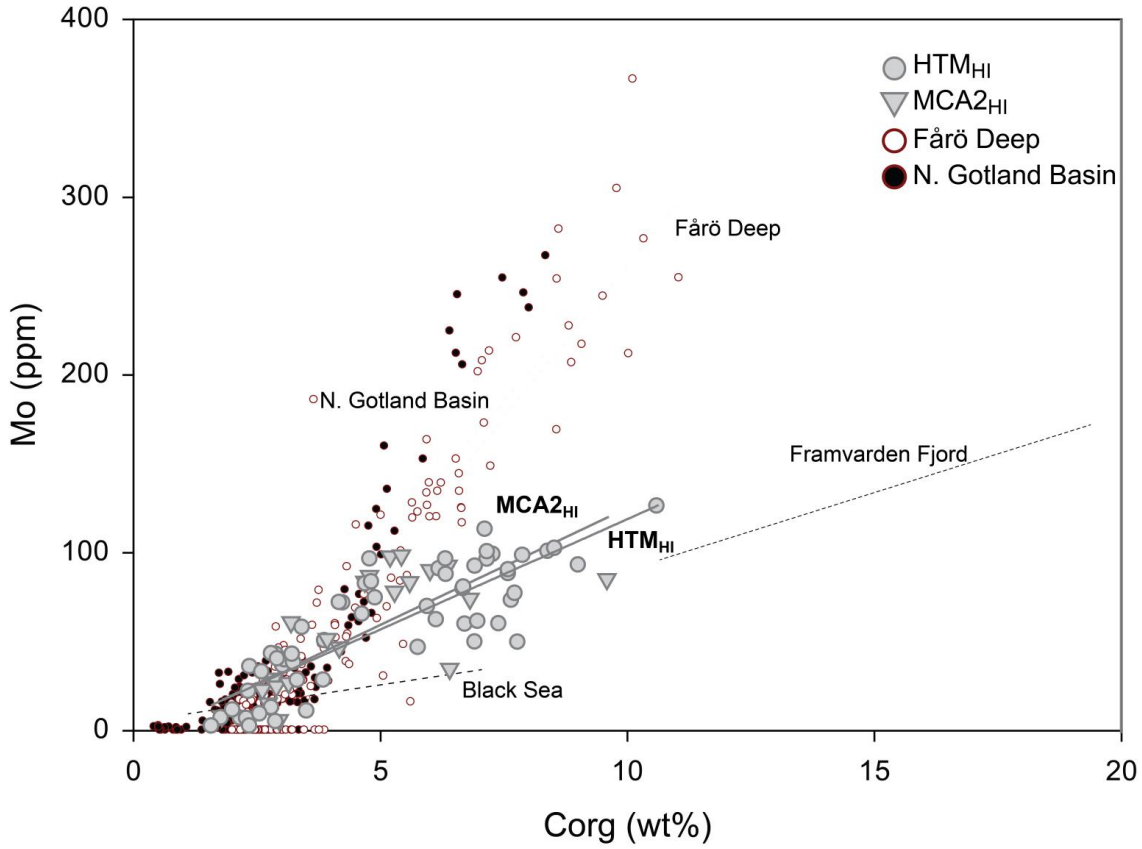

Figure S1: Organic carbon content (C_{org}) versus Mo gradients for several brackish/marine systems. The data for the Fårö Deep (site: F80) and the Northern Gotland Basin (site: LL19) are published in Jilbert and Slomp (2013b) (dotted red lines) whereas the data for the Framvaren Fjord and the Black Sea are summarized in Algeo and Lyons (2006) (dotted black lines). The data for the latter two basins are only presented as gradients. Only the data for two main hypoxic intervals in our sediment core from the Landsort Deep, the HTM_{HI} and $MCA2_{HI}$, are shown. The average slopes of the gradients for the HTM_{HI} and $MCA2_{HI}$ differ slightly (solid grey lines; 12.4 and 13.2, respectively).

S2: Depth profile of reactive Fe-oxides relative to Fe-bound P for Hole E.

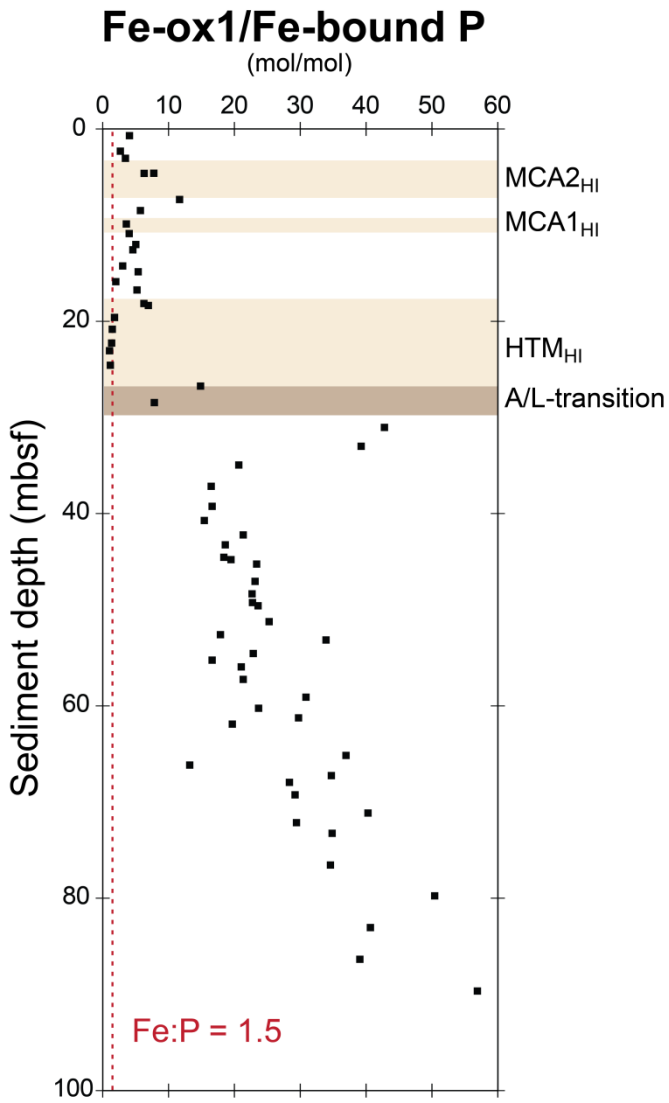

Figure S2: Depth profile of reactive Fe-oxides relative to Fe-bound P for Hole E. For details on the hypoxic intervals (HTM_{HI}, $MCA1_{HI}$ and $MCA2_{HI}$) and the A/L-transition: see caption of Fig. 2 and section 2.1. The ratios between the amorphous Fe-oxide content (Fe-ox1) and the Fe-bound P content are generally above 1.5 (Fe/P content in pure vivianite).

S3: Depth profiles of CDB-extractable Fe, Mn and Ca for Hole E

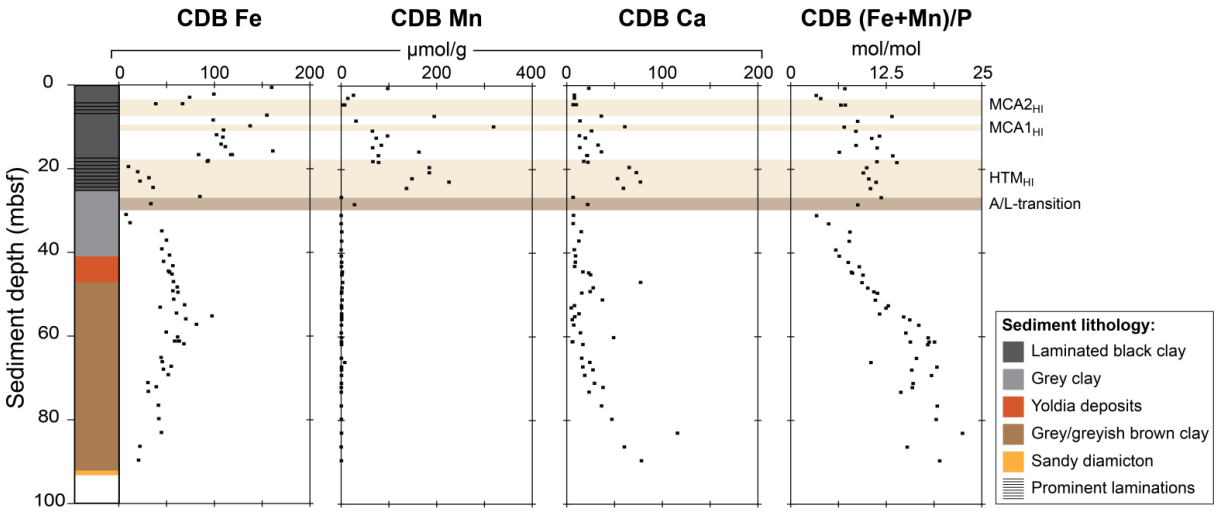

Figure S3: Depth profiles of CDB-extractable Fe, Mn and Ca for Hole E. Sediment lithology: see caption of Fig. 2. The Fe, Mn and Ca concentrations were measured by ICP-OES in the citrate-dithionite-bicarbonate (CDB) step of the SEDEX procedure (Ruttenberg, 1992). The ratios of Fe and Mn versus P in the CDB solutions are all above 1.5 mol/mol, implying that the CDB extracts contain sufficient Fe and Mn to explain all CDB-P as vivianite.

S4: Preferential release of phosphorus relative to carbon from organic matter

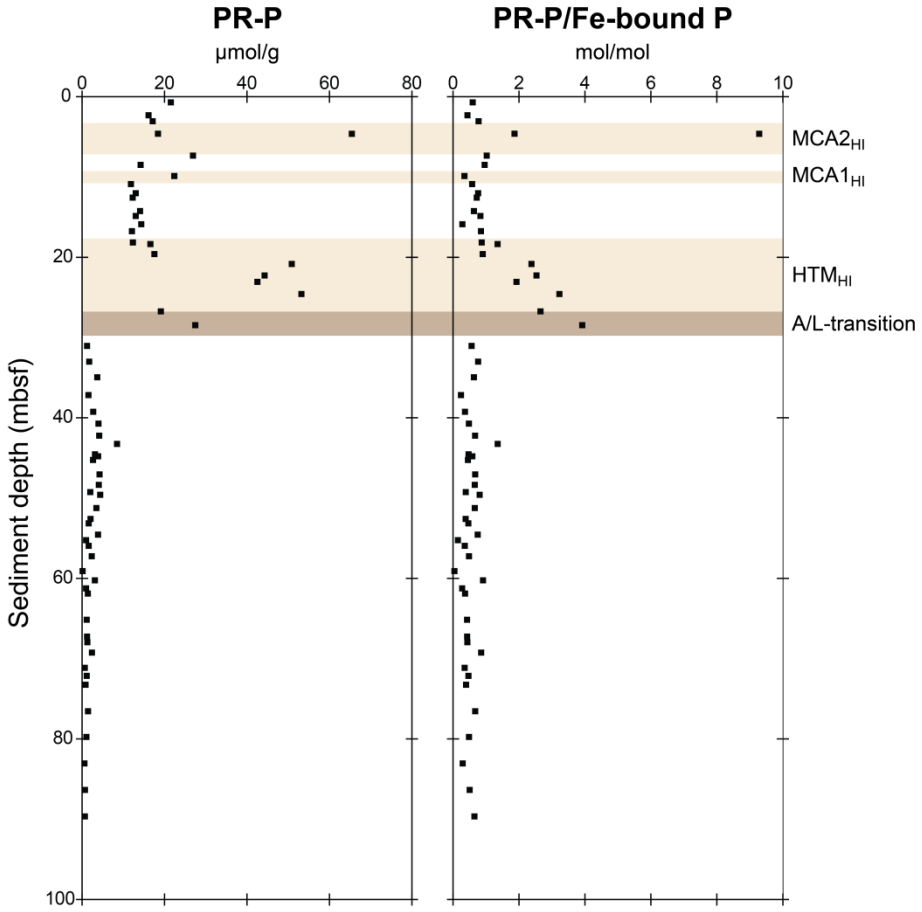

Figure S4: preferential release of phosphorus relative to carbon from organic matter. For details on the hypoxic intervals (HTM_{HI}, $MCA1_{HI}$ and $MCA2_{HI}$) and the A/L-transition: see caption of Fig. 2 and section 2.1. Preferentially released P (PR-P) is estimated by subtracting the current P content of the organic matter pool in the sediment ($P_{org\ (t=1)}$) from the original total organic P content ($P_{org(t=0)}$).

Released P = $P_{org(t=0)} - P_{org\ (t=1)}$

The latter is estimated by dividing the current organic C ($C_{org(t=1)}$) content by 106 (i.e. the C_{org}/P_{org} of marine planktonic organic matter):

$P_{org\ (t=0)} = C_{org(t=1)}/106$

S5: Total sedimentary Fe/Al versus Fe-bound P in the Littorina Sea sediments

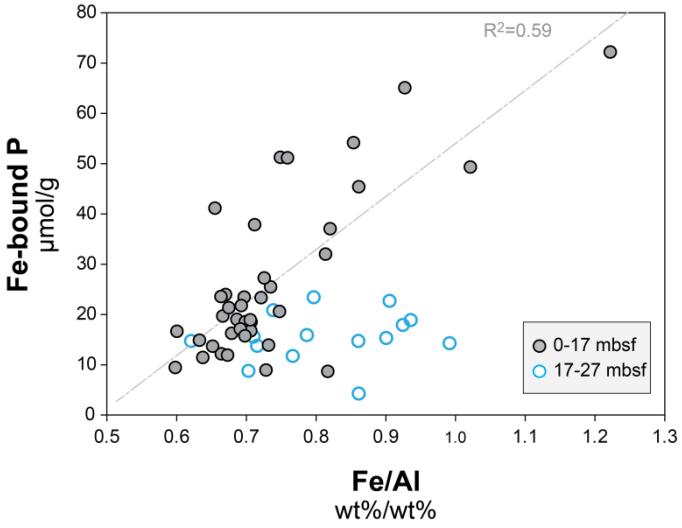

Figure S5: Total sedimentary Fe/Al versus Fe-bound P in the Littorina Sea sediments. A good correlation is observed in the Littorina Sea sediments from 0-17 mbsf including the $MCA1_{HI}$ and $MCA2_{HI}$ and the surrounding Littorina deposits (dotted grey line; Hole E and C). No clear correlation was observed between Fe/Al and Fe-bound P for the sediments between 17 and 27 mbsf (HTM_{HI} deposits; $R^2 = 0.03$)

S6: Depth profile of total S relative to reactive Fe for Hole E.

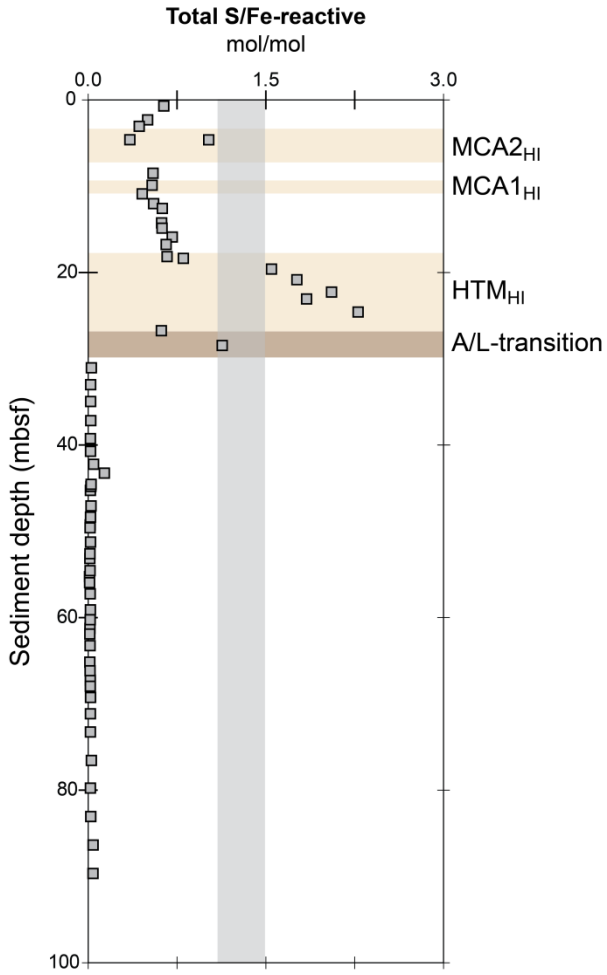

Figure S6: Depth profile of total S relative to reactive Fe for Hole E. For details on the hypoxic intervals (HTM_{HI}, $MCA1_{HI}$ and $MCA2_{HI}$) and the A/L-transition: see caption of Fig. 2 and section 2.1. The grey bar highlights values between 1.1 and 1.5. Sedimentary total S/Fe-reactive ratios below 1.5 are assumed to indicate that not all reactive Fe is captured as Fe-sulfides and vivianite formation is favoured (Rothe et al., 2015). The sediments in the study of Rothe et al. (2015) were all characterized by S:Fe-reactive ratios below 1.1 which may represent a more conservative threshold for vivianite occurrence. Reactive Fe is estimated as the sum of all Fe that is extracted in the Fe- and S-extractions.